A novel method for systematic genetic analysis and visualization of phenotypic heterogeneity applied to orofacial clefts

Jenna C. Carlson[1,2], Deepti Anand[3], Carmen J. Buxo[4], Kaare Christensen[5], Frederic Deleyiannis[6], Jacqueline T. Hecht[7], Lina M. Moreno[8], Ieda M. Orioli[9,10], Carmencita Padilla[11,12], John R. Shaffer[2,13], Alexandre R. Vieira[13], George L. Wehby[14], Seth M. Weinberg[2,13], Jeffrey C. Murray[15], Terri H. Beaty[16], Irfan Saadi[17], Salil A. Lachke[3,18], Mary L. Marazita[2,13], Eleanor Feingold[1,2], Elizabeth J. Leslie[19]*

1. Department of Biostatistics, Graduate School of Public Health, University of Pittsburgh, Pittsburgh, PA, 15261, USA
2. Department of Human Genetics, Graduate School of Public Health, University of Pittsburgh, Pittsburgh, PA, 15261, USA
3. Department of Biological Sciences, University of Delaware, Newark, DE 19716 USA
4. Dental and Craniofacial Genomics Core, School of Dental Medicine, University of Puerto Rico, San Juan, Puerto Rico, 00936, USA
5. Department of Epidemiology, Institute of Public Health, University of Southern Denmark, Odense, DK-5230, Denmark
6. Department of Surgery, Plastic and Reconstructive Surgery, University of Colorado School of Medicine, Denver, CO, 80045, USA
7. Department of Pediatrics, McGovern Medical School and School of Dentistry UT Health at Houston, Houston, TX, 77030, USA
8. Department of Orthodontics, College of Dentistry, University of Iowa, Iowa City, IA, 52242, USA
9. INAGEMP (National Institute of Population Medical Genetics), Porto Alegre, 91501-970, Brazil
10. ECLAMC (Latin American Collaborative Study of Congenital Malformations) at Department of Genetics, Federal University of Rio de Janeiro, Rio de Janeiro, 21941-902, Brazil
11. Department of Pediatrics, College of Medicine; Institute of Human Genetics, National Institutes of Health; University of the Philippines Manila, Manila, 1000, The Philippines
12. Philippine Genome Center, University of the Philippines System, Quezon City, 1101, The Philippines
13. Center for Craniofacial and Dental Genetics, Department of Oral Biology, School of Dental Medicine, University of Pittsburgh, Pittsburgh, PA, 15219, USA
14. Department of Health Management and Policy, College of Public Health, University of Iowa, Iowa City, IA, 52242, USA
15. Department of Pediatrics, Carver College of Medicine, University of Iowa, Iowa City, Iowa,52242, USA
16. Department of Epidemiology, Johns Hopkins Bloomberg School of Public Health, Baltimore MD, 21205, USA
17. Department of Anatomy and Cell Biology, University of Kansas Medical Center, Kansas City, KS 66160 USA
18. Center for Bioinformatics and Computational Biology, University of Delaware, Newark, DE 19716 USA
19. Department of Human Genetics, Emory University School of Medicine, Emory University, Atlanta, GA, 30322, USA

* Correspondence: ejlesli@emory.edu

Abstract

Phenotypic heterogeneity is a hallmark of complex traits, and genetic studies may focus on the trait as a whole or on individual subgroups. For example, in orofacial clefting (OFC), three subtypes – cleft lip (CL), cleft lip and palate (CLP), and cleft palate (CP) have variously been studied separately and in combination. It is more challenging, however, to dissect the genetic architecture and describe how a given locus may be contributing to distinct subtypes of a trait. We developed a framework for quantifying and interpreting evidence of subtype-specific or shared genetic effects in the study of complex traits. We applied this technique to create a "cleft map" of the association of 30 genetic loci with these three OFC subtypes. In addition to new associations with OFCs, we found loci with subtype-specific effects (e.g., *GRHL3* (CP), *WNT5A* (CLP), and *COL8A1* (CL)), as well as loci associated with two or all three subtypes. Within the *IRF6* and 8q24 loci, of which are both strongly associated with CL/P (CL with or without CP), we found multiple independent signals, including some with subtype-specific effects. We cross-referenced these results with mouse craniofacial gene expression datasets, which identified promising candidate genes. However, we found no strong correlation between OFC subtypes and gene expression patterns. In aggregate, the cleft map revealed that neither subtype-specific nor shared genetic effects operate in isolation in OFC architecture. Our approach can be easily applied to any complex trait with distinct phenotypic subgroups.

Author Summary

Orofacial clefts (OFCs), which include cleft lip and cleft palate, are the most common craniofacial birth defects in humans. Like many complex traits, OFCs exhibit striking phenotypic heterogeneity with three distinct anatomical subtypes (cleft lip, cleft lip and palate, and cleft palate). Despite the rapid pace of discovery of genetic variants influencing risk for OFC, how these variants influence these different OFC subtypes remains unknown. We developed a quantitative framework to interpret the evidence for subtype-specific or shared genetic effects for complex traits and applied it to 30 loci associated with OFCs. We found evidence for both subtype-specific genetic effects, as well as shared effects between two or all three subtypes, reflecting the complexity of genetic influences on risk to OFC. The results of this study will improve our ability to connect specific genetic variants to human phenotypes, understand the function of these genes and variants on craniofacial development, and pave the way for more predictive risk models.

Introduction

Most complex human traits (defined as those with both genetic and non-genetic risk factors) exhibit some phenotypic heterogeneity and variable expression with potentially hundreds of significantly associated genetic risk factors showing strong evidence of association (i.e. achieving genome-wide significance in large studies). Determining the relevance of any particular genetic risk factor at the individual or family level. is a significant challenge. There are several methods to compare correlated quantitative phenotypes, including those using a multivariate regression framework and the correlation between multiple phenotypes in cohorts or samples of cases and controls. However, these methods estimate statistical correlation to measure phenotype relatedness and are not suitable for examining mutually exclusive disease subtypes. Further, when these methods make comparisons based on the entire genome, which lacks the specificity of a more localized approach and could obscure biologically meaningful relationships.

We propose a targeted approach based on summary statistics from genome-wide association to sort out phenotypic heterogeneity. To illustrate this approach, we apply it to orofacial clefts (OFCs), congenital birth defects affecting the face and oral cavity. OFCs are the most common human craniofacial birth defect and combined they occur in approximately 1 in 800 live births worldwide [1]. Although there are many types of OFCs, the term is most commonly used to refer to clefts of the upper lip and/or palate. For our purposes, OFCs will refer to cleft lip (CL), cleft lip with cleft palate (CLP), or cleft palate (CP), the three most common types of OFCs. There is an additional combined category of CL with or without CP (CL/P), historically felt to be distinct from CP alone due to the separate embryological origins of the upper lip and secondary palate. Thus, within the CL/P group, CL and CLP have been considered variants of the same defect that only differed in severity [2].

Notably, more recent extensive epidemiological, genetic, and biological data suggest a more complex relationship between CL, CLP, and CP with both common and unique etiologic factors. In population-based studies in Denmark [3] and Norway [4], the recurrence risk for siblings was not uniform. The recurrence risks are consistently highest within the same subtype—for example an individual with CLP is more likely to have a sibling with CLP rather than CL or CP—supporting the possibility of subtype-specific effects. Further, "between-subtype" recurrence risks for CL and CLP—for example an individual with CL having a sibling with CLP or vice versa—are lower than within-subtype risks, but are not equal, lending support for the hypothesis that genetic risks for CL and CLP may differ. The lowest recurrence risks were "between-subtype" risks involving CP, but were still higher than the baseline risk in the general population, suggesting some shared etiology between CL/P and CP. In the case of multiplex OFC families, the affected individuals in such families most commonly all have CL/P or have CP. Notably, there are also mixed multiplex families with both CL/P and CP present among relatives, most commonly seen with syndromic forms of OFCs.

Taken together these observations imply a genetic predisposition for specific OFC subtypes, but there is limited genetic evidence supporting subtype-specific risk factors, especially for CL versus CLP. The primary focus of the OFC genetics literature has been on CL/P, where over 25 genetic risk loci have been identified to date from genome-wide studies, accounting for a modest portion (~30%) of the overall genetic variance for risk to CL/P [1, 5-8]. By contrast, only one locus has been identified for CP [9]. To date, subtype-specific associations are limited to three loci: 13q31 near *SPRY2* and *GREM1* (15q13) associated specifically with CLP [10-12], and *GRHL3* (1p36) associated with CP [9, 13]. There is some evidence that markers near *IRF6* (1q32) have a stronger effect on risk for CL than CLP, but this has not been consistently replicated [1, 14].

Given the growing body of evidence suggesting the presence of subtype-specific signals and the broader knowledge base of shared signals, we hypothesize neither type of statistical signal operates in isolation to affect craniofacial development. Rather, it is the combination of shared risk loci and perhaps subtype-specific risk loci affecting an individual's risk for OFC and their specific OFC subtype. In the current study, we sought to identify novel genetic risk variants for three specific OFC subtypes, CL, CLP, and CP, and examine all genetic risk loci for evidence of being specific to only one OFC subtype or of being shared between two or more subtypes of OFC.

Results/Discussion

Genome-wide meta-analysis of CL, CLP, and CP

First, we performed genome-wide meta-analyses for CL, CLP, and CP using imputed genotype data from the GENEVA and Pittsburgh Orofacial Cleft (POFC) consortia (Figure 1, Table S1). The GENEVA consortium used a family-based design and included 461 case-parent trios with CL, 1143 case-parent trios with CLP, and 451 case-parent trios with CP after removing individuals overlapping the two consortia. The POFC consortium included both a case-control arm and a case-parent trio arm, comprising 179 cases and 271 case-parent trios with CL, 644 cases and 1,048 case-parent trios with CLP, 78 cases and 165 case-parent trios with CP, plus 1,700 unaffected controls with no known family history of OFC drawn from the same populations as the unrelated cases. In the POFC case–control subgroup, we used logistic regression to test for association under an additive genetic model [15]. The two case-parent trio subgroups from POFC and GENEVA were analyzed separately using the allelic transmission disequilibrium test (TDT). The resulting effect estimates for the three analysis groups were combined using an inverse-variance weighted fixed-effects meta-analysis. This procedure was followed separately for genome-wide meta-analyses of CL and CLP (Figure S1); the results of the meta-analysis of CP was previously published [6] and are also depicted in Figure S1.

From these three analyses by cleft type, a total of 1,231 SNPs across 29 loci demonstrating suggestive evidence of association (i.e. $p<1.00\times10^{-5}$) in any of the three analyses were selected for further follow-up (Figure 1, Table S2). In addition to the 19 recognized risk loci previously reported in GWAS of CL/P or CP separately [6, 7], this study serves as independent replication for 17q21.3 (near *WNT9B* and *GOSR2*). Nine additional risk loci, although not reaching formal genome-wide significance, were suggested. Three of these—on 1p36.3, 3p14.3, and 5q35.2—have obvious candidate genes previously implicated in craniofacial development or in human craniofacial anomalies. At 1p36.3, a balanced translocation disrupting the *CAPZB* gene was reported in a patient with micrognathia and CP; subsequent studies showed capzb(-/-) zebrafish mutants recapitulated these human phenotypes [16]. The 5q35.2 signal is adjacent to *MSX2*, a gene critical for human skull development and associated with craniosynostosis, parietal foramina, and orofacial clefting [17]. Finally, the 3p14.3 locus had two independent signals within the same topologically-associated domain containing *WNT5A*, a gene in which mutations can cause mandibular hypoplasia in Robinow syndrome [18, 19] and *ERC2*, encoding a synapse protein [20]. As *WNT5A* is a stronger candidate gene for OFCs than *ERC2*, we represent the two signals as *WNT5A* “a” and *WNT5A* “b”.

Identification of independent signals

The 8q24 and *IRF6* loci represent large genomic intervals and have previously shown multiple, statistically independent associations with various OFC phenotypes, although the independence of signals has only been formally tested for the 8q24 gene desert region [15]. We separated SNPs into multiple groups based on LD “clumps” calculated with PLINK software [21]. In doing so, we confirmed the presence of multiple independent signals in the *IRF6* region and found evidence for a third signal at the 8q24 region (Figure S3). In total, three loci represented multiple independent signals—1q32 (*IRF6*), 8q24, and 3p14.3 (*WNT5A*)—thus the 29 associated loci comprised 34 independent signals.

Comparisons of CL, CLP, and CP

With 1,231 associated SNPs from the 34 independent signals revealed by our three meta-analyses, we used a heterogeneity Q-statistic [22] to compare effects for each SNP among subgroups to determine if any of these loci showed evidence of subtype-specific or shared risk (Figure 1). Specifically, effects of CL were compared to those of CLP, and the effects of CLP compared to those of CP. These contrasts were selected based on the biological plausibility of shared genetic effects between clefts affecting the lip (CL and CLP) and clefts affecting the palate (CLP and CP). To aid in the identification of subtype-specific variants, the direction of association was calculated by the difference in absolute values of the log odds ratios (i.e. $|\log(OR_{CLP})| - |\log(OR_{CL})|$, $|\log(OR_{CLP})| - |\log(OR_{CP})|$).

We sought to visually represent these findings so the evidence of subtype-specific effects become clear. Rather than dichotomizing genetic effects as “subtype-specific” or “shared”, we wanted to represent both the statistical evidence for heterogeneity and the overall statistical evidence of association with cleft subtypes for each locus. To this end, we developed a graphical representation, hereafter referred to as “the cleft map” to describe the statistical effect of numerous genetic loci on the architecture of OFCs. On the cleft map, the position of any single SNP is determined by the sum of two vectors, each given by the $-\log_{10}$ p-value of the heterogeneity Q-statistic times the sign of the direction of the locus (Figure 1). The position of a SNP thus represents how heterogeneous its estimated effects were between two cleft subtypes; SNPs further from the origin demonstrate more statistical evidence of heterogeneity. The x-axis of the cleft map represents the CL vs. CLP comparison and the y-axis represents the CLP vs. CP comparison.

When all SNPs for a locus were plotted, they generally clustered in specific locations based on the cleft type(s) with which the locus is associated (Figure 2, Figure S4). For example, SNPs located near the origin of the axes were those that showed less evidence of cleft-subtype

specificity. Such a pattern occurred for all 4 tested SNPs at the *FOXE1* locus (Figure 2A), consistent with existing literature indicating associations with all OFC subtypes [6, 23]. In contrast, all 13 SNPs at the *GRHL3* locus (Figure 2B) showed a significant CP-specific association ($p_{CLP.CP}<6.2\times10^{-5}$) and are positioned along the y-axis in the lower half of the map. Similarly, all 126 SNPs in the *IRF6* "a" locus (Figure 2C) showed a significant association with CL/P, as evidenced by significant differences in the CLP-CP comparison ($p_{CLP.CP}<6.9\times10^{-5}$), but there was no evidence of difference between CL and CLP ($p_{CLP.CL}>0.26$). The independent *IRF6* "a" and *IRF6* "b" regions contain rs2235371 [24] and rs642961, respectively. Previous studies suggested that rs642961 was preferentially associated with CL [14]. Although *IRF6* "b" SNPs show a quite complex relationship with different cleft types probably related to underlying differences in linkage disequilibrium (LD) (Figure S3), the location of the SNP cluster containing rs642961 in the upper-left quadrant of the cleft map supports a stronger effect on risk for CL compared to CLP (Figure 2D).

With a few exceptions, the tight clustering of SNPs allowed us to simplify the map by representing each locus region centered around its SNP cluster (Table 1, Figure 3). In addition to the loci described above, several others demonstrated some evidence of cleft subtype specificity including *MSX2* with CLP (Figure 2E, $p_{CLP.CP}<7.3\times10^{-4}$, $p_{CLP.CL}<5.6\times10^{-3}$), *WNT5A "a"* with CLP (Figure S4F, $p_{CLP.CP}<0.09$, $p_{CLP.CL}<1.1\times10^{-4}$), 9q21.32 with CL (Figure 2F, $p_{CLP.CP}=0.24$, $p_{CLP.CL}=4.06\times10^{-5}$), and 5p13.2 with CP (Figure S4K, $p_{CLP.CP}<2.2\times10^{-4}$).

Table 1. Summary of Cleft Map results for all 34 independent signals across 29 loci

Region	Candidate Gene(s)	CL vs. CLP		CLP vs. CP		Centroid Coordinates	N SNPs
		Min P_Q	Max P_Q	Min P_Q	Max P_Q		
1p36.13	PAX7	0.015	0.785	**7.65E-09**	0.014	0.9917,3.326	73
1p36.13	CAPZB	0.034	0.133	9.38E-04	5.00E-03	1.188,2.679	15
1p36.11	GRHL3	0.483	0.969	**1.36E-06**	**6.24E-05**	-0.191,-4.663	13
1p22	ARHGAP29	0.222	0.975	**6.26E-04**	0.159	0.1046,1.473	16
1q23.1	ETV3	0.010	0.014	0.057	0.068	1.914,1.214	6
1q32 "a"	IRF6	0.262	0.979	**1.78E-12**	**6.93E-05**	-0.0933,7.207	126
1q32 "b"	IRF6	5.46E-03	0.672	**1.18E-12**	2.16E-03	-1.199,5.751	58
1q32 "c"	IRF6	9.44E-02	0.994	**7.17E-09**	3.43E-02	0.1599,1.256	126
2p24.2	FAM49A	0.510	0.991	0.092	0.196	0.1883,0.8341	53
3p14.3 "a"	WNT5A	**8.19E-05**	**1.16E-04**	0.060	0.090	4.011,1.134	2
3p14.3 "b"	WNT5A	0.057	0.078	0.207	0.273	1.194,0.632	5
3q12.1	COL8A1, FILIP1L	2.72E-03	0.014	1.60E-03	0.054	-2.308,1.964	106
3q28	TP63	0.580	0.933	8.75E-03	0.018	-0.1078,1.871	5
4q21.1	SHROOM3	0.708	0.995	**5.20E-05**	2.95E-03	0.02269,3.2	13
5p13.2	CAPSL, SKP2	0.736	0.933	**2.00E-05**	**2.29E-04**	-0.03216,-4.047	4
5q35.2	MSX2	1.75E-03	0.006	**1.92E-04**	**7.36E-04**	2.421,3.437	8
6p22	TRIM10	0.332	0.332	0.361	0.361	0.4784,0.4425	1
8q21	DCAF4L2, MMP16	0.305	0.916	1.59E-03	0.254	0.1946,1.609	10
8q22.3	FZD6, RIMS2	0.012	0.012	0.136	0.136	1.931,0.8674	1
8q24 "a"		0.237	0.974	**2.10E-09**	0.003	-0.2666,5.396	57
8q24 "b"		2.87E-03	0.992	**3.72E-07**	0.088	-0.7306,3.179	108
8q24 "c"		0.092	0.980	**7.02E-05**	0.024	0.1114,2.671	94
9q21.32	TLE1	**4.06E-05**	**4.06E-05**	0.240	0.240	-4.391,-0.6196	1
9q22	FOXE1	0.602	0.708	0.227	0.271	0.174,-0.593	4
10q25	VAX1, SHTN1	0.316	0.921	0.179	0.415	0.2362,0.5786	22
12q13	KRT8, KRT18	0.088	0.573	**1.10E-05**	1.50E-03	0.5406,3.777	12
13q31	SPRY2	0.096	0.447	**9.08E-05**	1.36E-03	0.7439,3.599	10

13q32.3	CLYBL, ZIC5, ZIC2	0.109	0.271	0.062	0.586	0.7145,0.8081	13
15q22.2	TPM1	0.261	0.261	0.059	0.059	0.5834,1.231	1
15q24.1	ARID3B	0.519	1.000	3.61E-03	0.015	0.08757,2.12	137
17p13	NTN1	0.020	0.953	**1.28E-06**	0.391	0.6106,2.531	42
17q21.32	WNT9B	0.357	0.707	0.239	0.704	0.3152,0.3496	39
17q22	NOG	0.460	0.475	**1.26E-06**	**7.56E-06**	-0.3303,-0.3891	2
20q12	MAFB	0.071	1.000	2.13E-03	0.389	0.6294,1.634	42

Expression analyses in associated loci

Above we have referred to each associated locus by either a plausible candidate gene (e.g., *IRF6*) based on the literature on OFCs and craniofacial development or as a genetic location (e.g., 8q24) for gene deserts or new loci. Although this comports with the standards of the field, recent work demonstrates that disease-associated variants can regulate distant genes, suggesting that the nearby genes prioritized by GWAS may not always be involved [25, 26]. In addition, multiple genes in a given region may be co-regulated and expressed in similar tissues or expressed in distinct compartments within the craniofacial complex [27]. We, therefore, wanted to agnostically explore gene expression profiles of all genes contained in these regions to determine if their expression profiles could explain clustering of associated genes or provide mechanistic insights into the pathogenesis of OFC subtypes.

We first identified all of the genes located in the same topologically associated domains (TADs), because the associated SNPs may have regulatory functions and there is evidence that such SNPs are more likely to act upon genes located within their own TAD (Table S3) [28]. We used published topological data from human embryonic stem cells because although there are no known craniofacial-specific TADs, boundaries are largely conserved across cell types [29]. To prioritize highly expressed genes, we identified those genes with mouse homologs reported to be differentially expressed among several transcriptomic datasets from key periods, regions,

and tissues in mouse facial development [30]. Hooper et al. previously integrated these datasets with a weighted gene co-expression network analysis to generate 75 co-expression modules describing gene expression in the developing mouse face. We used these modules to annotate each gene in our list (Table S4). Of the 222 homologs in our 29 loci, 101 (45.44%) were present among these co-expression modules. Each region contained at least one gene assigned to a co-expression module, but only seven regions contained a single gene or only one gene with documented craniofacial expression (Figure S5). Overall, this is not surprising given these co-expression modules contained over 8,000 genes, or approximately 30% of the mouse genome.

To further refine the possible candidate genes, we turned to a complementary resource of gene expression profiles, SysFACE (Systems tool for craniofacial expression-based gene discovery) (Table S5) [31], which allows easy visualization of data from orofacial tissue microarrays or RNA-seq datasets for mandible, maxilla, frontonasal prominence, and palate, collected largely as part of the FaceBase consortium [32, 33]. We used SysFACE to examine enriched craniofacial expression by comparing orofacial tissue data with embryonic whole body tissue [34]. For most loci, the SysFace analysis corroborated the co-expression modules or prioritized one gene. For example, at the *PAX7* locus, although three genes (*Pax7, Klhdc7a*, and *Aldh4a1*) were found in craniofacial co-expression modules only *Pax7* showed strong enrichment in SysFACE.

For the six new loci without any clear candidate genes (5p13.2, 6p22, 8q22.3, 9q21.32, 13q32.3), we used both datasets to identify likely candidate genes. At the 5p13.2 locus, *Skp2* was present in the mesenchyme expression module and showed high SysFACE scores across multiple processes in the microarray data and RNA-seq expression in the palate. Other genes (*Capsl* and *Slc1a3*) were in the ectoderm module with enriched expression in the palate. Because this locus is associated only with CP, any or all of these genes could be relevant. At the 6p22 and 8q22.3 loci, multiple genes were found in both the Hooper and SysFACE

datasets, but were expressed in different expression modules. Although *FZD6* (8q22.3) was previously implicated in CLP by linkage in a large multiplex CLP family, as well as by craniofacial anomalies observed in a *fzd6* morphant [35], it is possible multiple genes contribute to the association signals at these loci. In sum, each newly associated locus contained one or more genes with craniofacial expression; detailed *in vivo* analyses will be required to pinpoint specific causal genes.

We performed an enrichment analysis for the set of genes present in these co-expression modules. These genes were enriched for broad biological processes such as “embryonic morphogenesis”, “epithelium development” and human and mouse phenotypes related to OFCs, including “oral cleft”, “perinatal lethality”, “abnormal craniofacial morphology”. Unfortunately, the broad terms from the enrichment analysis did not support more specific hypotheses about the pathogenesis of OFCs. The co-expression modules revealed a critical role for ectodermal genes in OFC pathogenesis, and fewer loci with mesenchymally-expressed genes. However, most genes were broadly expressed across multiple facial prominences, limiting our ability to hypothesize about any one mechanism for how these genes relate to OFC subtypes, but these tools will be useful for prioritizing genes for future association studies. A few genes, however, had very specific expression patterns worthy of further discussion. As one example, *PAX7* expression was restricted to the frontonasal prominence, whereas other loci (i.e., *SPRY2*, *MSX2*) that clustered nearby in the cleft map showing stronger evidence of effects on risk for CLP were more broadly expressed in the maxilla and mandible. Similarly, the *COL8A1* locus showed a stronger effect on CL than CLP, but was still very strongly expressed in the palate. Interestingly, *Col8a1* expression was enriched early at E10.5 in the frontonasal and maxillary prominences, when lip fusion takes place. These patterns are consistent with the direction of the SNP effects at this locus where the same alleles conferred a protective effect (OR < 1) for CL and CLP scans, but a modest, (and not formally significant) risk effect (OR > 1) in the CP scan.

Thus, our data argue both the early expression and the palatal expression are important. It is possible that the as-yet-unknown functional SNPs could promote palatal fusion and protect against a CP; alternatively, they could dysregulate *COL8A1* promoting ectopic expression in the lip. Our current study cannot definitively answer these questions, but by demonstrating this locus may exert a stronger effect on risk to CL while the gene is expressed in the palate, it could motivate more targeted follow-up studies.

In our statistical analyses, we observed most of the loci previously identified in CL/P GWAS were positioned along the y-axis, indicating that there was no statistical difference between CL and CLP. This is not surprising, as a combined study of CL and CLP has the greatest power to identify loci with similar effects in both of these subgroups. One limitation of this study is that we did not capture several loci discovered in previous CL/P GWAS (e.g., *RHPN2* [15]) because no SNP showed p-values better than 10^{-5}. As these loci were found only in the combined CL/P group, we would expect them to be positioned along the y-axis. Such SNPs show the statistical power of traditional analyses of CL/P, which have been successful. However, our study also demonstrates there are multiple loci with subtype-specific effects (e.g. *WNT5A*) or with stronger effects for CL than CLP (e.g. *COL8A1*) that are more difficult to detect in the combined analyses.

An important contribution of this work was the careful examination of the three large loci with multiple, independent signals based on LD. Of these, we found evidence for independent signals within *WNT5A* and *IRF6* exerting potentially different effects between subtypes. In contrast, the three 8q24 signals were largely overlapping and associated with the combined phenotype CL/P (Figure S2 M-O); only the 8q24 “c” signal showed even marginal evidence of a stronger effect with CL than CLP. At the *IRF6* locus, the “b” signal was tagged by rs642961, a SNP that disrupts the binding site of TFAP2α in the MCS9.7 enhancer [14]. However, MCS9.7 activity did not completely recapitulate endogenous *IRF6* activity, most notably in the medial-

edge epithelium during palatal fusion, indicating the presence of some other enhancer [36]. Similarly, the 8q24 gene desert contains multiple craniofacial enhancers [27] which influence *Myc* expression [37]. Such enhancers are known to have restricted activity patterns and often act in a modular fashion to control gene expression by activating expression in different anatomical regions or at different points during development [38]. These characteristics present a logical mechanism to drive phenotypic heterogeneity. Understanding the logic of these enhancers, the function of SNPs within them, and the relationship between risk alleles and disease subtypes will be critical for fully understanding the etiology of OFCs.

Our approach works well to describe SNPs and loci where the direction of the effect is the same among subtypes. However, when the odds ratios exhibit different effect directions, the log odds ratios may be close in value, and the sign representing the direction of the effect may fluctuate according to the subtype with a slightly larger effect at any given SNP. One can diagnose these cases by plotting estimated effects of the individual SNPs, resulting in two clusters of SNPs on opposite ends of the plot (as seen in Figure S4Z). Overall, plotting the centroid (as shown for the *NOG* locus (Figure S4AA)) most closely represents the overall picture of the locus—i.e. that there isn't an association with one particular cleft type. However, if an allele truly increases risk for one cleft type and reduces risk for another, as was recently reported for *NOG* [39], we may be obscuring biologically meaningful results. Similarly, there is a set of SNPs within *IRF6* "c" (apparently independent of the *IRF6* "a" and *IRF6* "b" signals), with p-values in the CP meta-analysis of ~8×10^{-3} and whose minor alleles appear to increase risk for CP; these same alleles appear to decrease risk for CL/P. Although genetic association studies overwhelmingly support an association between common SNPs in *IRF6* and risk of CL/P, dominant mutations in the gene cause Van der Woude syndrome, recognized as one of few syndromes where both CL/P and CP occur within the same family. With this new information about this locus, it may be time

to revisit the idea that common SNPs within this locus could act as modifiers of which OFC phenotype appears in Van der Woude families [40].

In summary, we developed a novel approach for dissecting the genetic contribution to phenotypic heterogeneity of OFCs. We identified novel genetic associations, some of which, like *MSX2*, showed evidence of subtype specificity, and would have been missed by traditional analyses where all subtypes are combined. Three loci, *IRF6*, *WNT5A*, and 8q24 represent multiple independent signals. Ours is the first study to formally confirm multiple signals from *IRF6* locus, which had been suggested previously [14]. Importantly, some of these signals showed different effects on the different OFC subtypes, adding an additional layer of complexity to the genetic architecture of this most common group of craniofacial malformatons. Finally, cross-referencing our results with gene expression data has generated new hypotheses about mechanisms by which OFC subtypes may occur. However, genetic studies alone are unlikely to completely elucidate the etiology of OFCs or other complex traits. Here, we focused only on fetal contributors to OFC risk, but the etiology of this disorder likely includes significant environmental components, epigenetic factors, parent-of-origin effects, stochastic processes, or additional genetic modifiers. With respect to OFCs, we have previously shown evidence of both common and rare [41] genetic modifiers possibly distinguishing between CL from CLP. Our approach may serve to guide targeted tests for gene-gene interaction and risk score analyses to further disentangle the complex etiologic architecture of OFCs. Future extensions of this approach can incorporate these modifiers and interactions, and can examine other subtype definitions, other structural birth defects, or any other complex trait with phenotypic heterogeneity where subtypes can be delineated. Finally, we note our approach uses only GWAS or candidate gene study summary statistics, so information from multiple studies can more easily be leveraged to dissect the complex architecture of heterogeneous traits.

Methods

Contributing GWAS studies

Two consortia contributed to this study. The first, from the GENEVA consortium, used a family-based design and included 461 case-parent trios with cleft lip (CL), 1,143 case-parent trios with cleft lip and palate (CLP), and 451 case-parent trios with CP, respectively, from populations in Europe (Denmark and Norway), the United States, and Asia (Singapore, Taiwan, Philippines, Korea, and China). The specifics of this study have been described previously [9, 15, 42]. Briefly, samples were genotyped for 589,945 SNPs on the Illumina Human610-Quadv.1_B BeadChip, genetic data were phased using SHAPEIT, and imputation was performed with IMPUTE2 software to the 1000 Genomes Phase 1 release (June 2011) reference panel. Genotype probabilities were converted to most-likely genotype calls with the GTOOL software (http://www.well.ox.ac.uk/~cfreeman/software/gwas/gtool.html).

The second consortium included samples from the Pittsburgh Orofacial Cleft (POFC) study, comprising 179 cases and 271 case-parent trios with CL, 644 cases and 1,048 trios with CLP, 78 cases and 165 trios with CP, and 1,700 unaffected controls with no history of craniofacial anomalies. Participants were recruited from 13 countries in North America (United States), Central or South America (Guatemala, Argentina, Colombia, Puerto Rico), Asia (China, Philippines), Europe (Denmark, Turkey, Spain), and Africa (Ethiopia, Nigeria). Additional details on recruitment, genotyping, and quality controls were previously described [9, 15]. Briefly, these samples were genotyped for 539,473 SNPs on the Illumina HumanCore+Exome array. Data were phased with SHAPEIT2 and imputed using IMPUTE2 to the 1000 Genomes Phase 3 release (September 2014) reference panel. The most-likely genotypes (i.e. genotypes with the highest probability [Q]) were selected for statistical analysis only if the genotype with the highest probability was greater than 0.9.

A total of 412 individuals were in both the GENEVA OFC and POFC studies, so we excluded these participants from the GENEVA study for this analysis. Informed consent was obtained for all participants and all sites had both local IRB approval and approval at the University of Pittsburgh, the University of Iowa, or Johns Hopkins University. Individual level genotype and phenotype data for the GENEVA and POFC studies are available from dbGaP: phs000774.v1.p1 and phs000094.v1.p1.

Genome-wide meta-analyses for CL, CLP, and CP

We previously described our methods for quality control and meta-analysis of the GENEVA OFC and POFC studies [6]. GWAS was performed for CL, CLP, and CP separately on SNPs with minor allele frequencies (MAF) greater than 1% and not deviating from Hardy-Weinberg Equilibrium (HWE $p > 0.0001$) in the parents or control subjects. Tests of association using unrelated cases and controls matched for population of origin used logistic regression models, while case-parent trios were analyzed with or the allelic transmission disequilibrium test (TDT) implemented in PLINK. Within each OFC subtype, the resulting effects estimates were combined in an inverse-variance weighted fixed-effects meta-analysis. The combined estimate, a weighted log odds ratio, should follow a chi-squared distribution with two degrees of freedom under the null hypothesis of no association.

Comparisons of cleft types

From the three meta-analyses, SNPs demonstrating suggestive evidence of association (i.e. $p < 1.00\times10^{-5}$) in any scan were considered for further analysis. For each SNP, two heterogeneity Q-statistics were calculated to compare effects of CL to CLP, and CLP to CP [22]. The magnitude of the log odds ratios for these two cleft subtypes were also compared to indicate the direction of effect (i.e. which subtype showed a stronger effect). Together, the Q-statistics and directions of effect for the two comparisons (CL to CLP, CLP to CP) prescribe a point for each

SNP on the cleft map. For each region, the centroid of these points was calculated to inform the overall effect of the locus.

SysFACE: mouse orofacial transcriptome data analysis

Mouse orthologs of human candidate genes were analyzed for their absolute expression and enriched expression in orofacial tissue microarray datasets on the Affymetrix 430 2.0 platform (GeneChip Mouse Genome 430 2.0 Array) deposited in NCBI GEO (https://www.ncbi.nlm.nih.gov/geo/) and FaceBase (https://www.facebase.org) (Table S5). Enriched expression was estimated by comparing orofacial tissue data with whole embryonic body tissue (WB) reference control obtained from series (GSE32334) as previously described [34]. Datasets for mandible (mouse embryonic stages E10.0, E10.5, E11.0, E11.5, E12.0, E12.5), maxilla (E10.5, E11.0, E11.5, E12.0, E12.5,) and frontonasal (E10.5, E11.0, E11.5, E12.0, E12.5) were obtained from the series GSE7759. Palate datasets were obtained for mouse E13.5 (FaceBase series: FB00000468.01), E14.5 (FB00000474.01, GSE11400) and P0 (GSE31004). RNA-seq data on Illumina HiSeq2500 platform for mouse E14.5 posterior oral palate (FB00000768.01), anterior oral palate (FB00000769.01) and WB (whole body, unpublished) were also used. 'R' statistical environment (http://www.r-project.org/) was used to import raw microarray datafiles on Affymetrix 430 2.0 platform, followed by background correction and normalization using Affy package [43] available at Bioconductor (www.bioconductor.org). Using a AffyBatch function, present/absent calls for probe sets were calculated and those with the highest median expression at significant p-values were collapsed into genes [43]. Differential gene expression (DEGs) and enrichment scores for all four orofacial tissues compared to WB were calculated using limma [44], and the detailed microarray workflow is described elsewhere [45]. RNA-seq data on Illumina HiSeq2500 platform were first subjected to quality control analysis for reads by using FastQC (http://www.bioinformatics.babraham.ac.uk/projects/fastqc/), and then subjected to sequence

trimming and clipping using Trimmomatic [46] with in house scripts (https://github.com/atulkakrana/preprocess.seq) [47]. Reads were aligned against the *Mus musculus* reference genome using TopHat v2.0.9 [48] with recommended settings. Transcript assembly for measuring relative abundances was performed using Cufflinks v2.1.1 [48]. After merging the assemblies by the function Cuffmerge, DEGs were identified using the Cuffdiff function [48]. Statistically significant DEGs (comparison of orofacial datasest with WB) were identified using an in-house Python script.

Acknowledgments

We thank the study participants for their enthusiastic participation and acknowledge the local recruitment staff and collaborators for their tireless efforts that made this study.

Funding Statement

This work was funded by grants from the National Institutes of Health: R00-DE025060 [EJL], R03-DE024776 [SAL, IS], X01-HG007485 [MLM, EF], R01-DE016148 [MLM., SMW], R01-DE009886 [MLM], R21-DE016930 [MLM], R01-DE014667 [LMM], R01-DE012472 [MLM], R01-DE011931 [JTH], R01-DE011948 [KC], R37-DE008559 (JCM, MLM), U01-DD000295 [GLW], K99-DE024571 [CJB], S21-MD001830 [CJB], U54-MD007587 [CJB], R01-DE014581 [TB], U01-DE018993 [TB]. Genotyping and data cleaning were provided via an NIH contract to the Johns Hopkins Center for Inherited Disease Research: HHSN268201200008I. The funders had no role in study design, data collection and analysis, decision to publish, or preparation of the manuscript.

References

1. Leslie EJ, Marazita ML. Genetics of cleft lip and cleft palate. American journal of medical genetics Part C, Seminars in medical genetics. 2013;163C(4):246-58. Epub 2013/10/15. doi: 10.1002/ajmg.c.31381. PubMed PMID: 24124047; PubMed Central PMCID: PMCPMC3925974.

2. Marazita ML. The evolution of human genetic studies of cleft lip and cleft palate. Annu Rev Genomics Hum Genet. 2012;13:263-83. Epub 2012/06/19. doi: 10.1146/annurev-genom-090711-163729. PubMed PMID: 22703175; PubMed Central PMCID: PMCPMC3760163.

3. Grosen D, Chevrier C, Skytthe A, Bille C, Molsted K, Sivertsen A, et al. A cohort study of recurrence patterns among more than 54 000 relatives of oral cleft cases in Denmark: support for the multifactorial threshold model of inheritance. Journal of medical genetics. 2010;47(3):162-8. Epub September 14, 2009. doi: 10.1136/jmg.2009.069385. PubMed PMID: WOS:000275771600004.

4. Sivertsen A, Wilcox AJ, Skjaerven R, Vindenes HA, Abyholm F, Harville E, et al. Familial risk of oral clefts by morphological type and severity: population based cohort study of first degree relatives. BMJ (Clinical research ed. 2008;336(7641):432-4. Epub 2008/02/06. doi: 10.1136/bmj.39458.563611.AE. PubMed PMID: 18250102; PubMed Central PMCID: PMCPMC2249683.

5. Dixon MJ, Marazita ML, Beaty TH, Murray JC. Cleft lip and palate: understanding genetic and environmental influences. Nat Rev Genet. 2011;12(3):167-78. Epub 2011/02/19. doi: 10.1038/nrg2933. PubMed PMID: 21331089; PubMed Central PMCID: PMCPMC3086810.

6. Leslie EJ, Carlson JC, Shaffer JR, Butali A, Buxo CJ, Castilla EE, et al. Genome-wide meta-analyses of nonsyndromic orofacial clefts identify novel associations between FOXE1 and all orofacial clefts, and TP63 and cleft lip with or without cleft palate. Hum Genet. 2017;136(3):275-86. Epub 2017/01/06. doi: 10.1007/s00439-016-1754-7. PubMed PMID: 28054174; PubMed Central PMCID: PMCPMC5317097.

7. Yu Y, Zuo X, He M, Gao J, Fu Y, Qin C, et al. Genome-wide analyses of non-syndromic cleft lip with palate identify 14 novel loci and genetic heterogeneity. Nature communications. 2017;8:14364. Epub 2017/02/25. doi: 10.1038/ncomms14364. PubMed PMID: 28232668; PubMed Central PMCID: PMCPMC5333091.

8. Ludwig KU, Bohmer AC, Bowes J, Nikolic M, Ishorst N, Wyatt N, et al. Imputation of orofacial clefting data identifies novel risk loci and sheds light on the genetic background of cleft lip +/- cleft palate and cleft palate only. Hum Mol Genet. 2017;26(4):829-42. Epub 2017/01/15. doi: 10.1093/hmg/ddx012. PubMed PMID: 28087736; PubMed Central PMCID: PMCPMC5409059.

9. Leslie EJ, Liu H, Carlson JC, Shaffer JR, Feingold E, Wehby G, et al. A Genome-wide Association Study of Nonsyndromic Cleft Palate Identifies an Etiologic Missense Variant in GRHL3. Am J Hum Genet. 2016;98(4):744-54. Epub 2016/03/29. doi: 10.1016/j.ajhg.2016.02.014. PubMed PMID: 27018472; PubMed Central PMCID: PMCPMC4833215.

10. Ludwig KU, Mangold E, Herms S, Nowak S, Reutter H, Paul A, et al. Genome-wide meta-analyses of nonsyndromic cleft lip with or without cleft palate identify six new risk loci. Nat

Genet. 2012;44(9):968-71. Epub 2012/08/07. doi: 10.1038/ng.2360. PubMed PMID: 22863734; PubMed Central PMCID: PMCPMC3598617.

11. Jia Z, Leslie EJ, Cooper ME, Butali A, Standley J, Rigdon J, et al. Replication of 13q31.1 association in nonsyndromic cleft lip with cleft palate in Europeans. Am J Med Genet A. 2015;167A(5):1054-60. Epub 2015/03/20. doi: 10.1002/ajmg.a.36912. PubMed PMID: 25786657; PubMed Central PMCID: PMCPMC4402974.

12. Ludwig KU, Ahmed ST, Bohmer AC, Sangani NB, Varghese S, Klamt J, et al. Meta-analysis Reveals Genome-Wide Significance at 15q13 for Nonsyndromic Clefting of Both the Lip and the Palate, and Functional Analyses Implicate GREM1 As a Plausible Causative Gene. PLoS Genet. 2016;12(3):e1005914. Epub 2016/03/12. doi: 10.1371/journal.pgen.1005914. PubMed PMID: 26968009; PubMed Central PMCID: PMCPMC4788144.

13. Mangold E, Bohmer AC, Ishorst N, Hoebel AK, Gultepe P, Schuenke H, et al. Sequencing the GRHL3 Coding Region Reveals Rare Truncating Mutations and a Common Susceptibility Variant for Nonsyndromic Cleft Palate. Am J Hum Genet. 2016;98(4):755-62. Epub 2016/03/29. doi: 10.1016/j.ajhg.2016.02.013. PubMed PMID: 27018475; PubMed Central PMCID: PMCPMC4833214.

14. Rahimov F, Marazita ML, Visel A, Cooper ME, Hitchler MJ, Rubini M, et al. Disruption of an AP-2alpha binding site in an IRF6 enhancer is associated with cleft lip. Nat Genet. 2008;40(11):1341-7. Epub 2008/10/07. doi: 10.1038/ng.242. PubMed PMID: 18836445; PubMed Central PMCID: PMCPMC2691688.

15. Leslie EJ, Carlson JC, Shaffer JR, Feingold E, Wehby G, Laurie CA, et al. A multi-ethnic genome-wide association study identifies novel loci for non-syndromic cleft lip with or without cleft palate on 2p24.2, 17q23 and 19q13. Hum Mol Genet. 2016;25(13):2862-72. Epub 2016/04/02. doi: 10.1093/hmg/ddw104. PubMed PMID: 27033726; PubMed Central PMCID: PMCPMC5181632.

16. Mukherjee K, Ishii K, Pillalamarri V, Kammin T, Atkin JF, Hickey SE, et al. Actin capping protein CAPZB regulates cell morphology, differentiation, and neural crest migration in craniofacial morphogenesisdagger. Hum Mol Genet. 2016;25(7):1255-70. Epub 2016/01/14. doi: 10.1093/hmg/ddw006. PubMed PMID: 26758871; PubMed Central PMCID: PMCPMC4787901.

17. Wilkie AO, Tang Z, Elanko N, Walsh S, Twigg SR, Hurst JA, et al. Functional haploinsufficiency of the human homeobox gene MSX2 causes defects in skull ossification. Nat Genet. 2000;24(4):387-90. Epub 2000/03/31. doi: 10.1038/74224. PubMed PMID: 10742103.

18. Person AD, Beiraghi S, Sieben CM, Hermanson S, Neumann AN, Robu ME, et al. WNT5A mutations in patients with autosomal dominant Robinow syndrome. Dev Dyn. 2010;239(1):327-37. Epub 2009/11/18. doi: 10.1002/dvdy.22156. PubMed PMID: 19918918; PubMed Central PMCID: PMCPMC4059519.

19. Hosseini-Farahabadi S, Gignac SJ, Danescu A, Fu K, Richman JM. Abnormal WNT5A Signaling Causes Mandibular Hypoplasia in Robinow Syndrome. J Dent Res. 2017;96(11):1265-72. Epub 2017/07/01. doi: 10.1177/0022034517716916. PubMed PMID: 28662348.

20. Ohtsuka T, Takao-Rikitsu E, Inoue E, Inoue M, Takeuchi M, Matsubara K, et al. Cast: a novel protein of the cytomatrix at the active zone of synapses that forms a ternary complex with RIM1 and munc13-1. J Cell Biol. 2002;158(3):577-90. Epub 2002/08/07. doi: 10.1083/jcb.200202083. PubMed PMID: 12163476; PubMed Central PMCID: PMCPMC2173811.

21. Purcell S, Neale B, Todd-Brown K, Thomas L, Ferreira MA, Bender D, et al. PLINK: a tool set for whole-genome association and population-based linkage analyses. Am J Hum Genet. 2007;81(3):559-75. Epub 2007/08/19. doi: 10.1086/519795. PubMed PMID: 17701901; PubMed Central PMCID: PMCPMC1950838.

22. Schenker N, Gentleman JF. On Judging the Significance of Differences by Examining the Overlap Between Confidence Intervals. The American Statistician. 2001;55(3):182-6.

23. Moreno LM, Mansilla MA, Bullard SA, Cooper ME, Busch TD, Machida J, et al. FOXE1 association with both isolated cleft lip with or without cleft palate, and isolated cleft palate. Hum Mol Genet. 2009;18(24):4879-96. Epub 2009/09/26. doi: 10.1093/hmg/ddp444. PubMed PMID: 19779022; PubMed Central PMCID: PMCPMC2778374.

24. Zucchero TM, Cooper ME, Maher BS, Daack-Hirsch S, Nepomuceno B, Ribeiro L, et al. Interferon regulatory factor 6 (IRF6) gene variants and the risk of isolated cleft lip or palate. N Engl J Med. 2004;351(8):769-80. Epub 2004/08/20. doi: 10.1056/NEJMoa032909. PubMed PMID: 15317890.

25. Smemo S, Tena JJ, Kim KH, Gamazon ER, Sakabe NJ, Gomez-Marin C, et al. Obesity-associated variants within FTO form long-range functional connections with IRX3. (1476-4687 (Electronic)).

26. Gupta RM, Hadaya J, Trehan A, Zekavat SM, Roselli C, Klarin D, et al. A Genetic Variant Associated with Five Vascular Diseases Is a Distal Regulator of Endothelin-1 Gene Expression. (1097-4172 (Electronic)).

27. Attanasio C, Nord AS, Zhu Y, Blow MJ, Li Z, Liberton DK, et al. Fine tuning of craniofacial morphology by distant-acting enhancers. Science. 2013;342(6157):1241006. Epub 2013/10/26. doi: 10.1126/science.1241006. PubMed PMID: 24159046; PubMed Central PMCID: PMCPMC3991470.

28. Dekker J, Marti-Renom Ma Fau - Mirny LA, Mirny LA. Exploring the three-dimensional organization of genomes: interpreting chromatin interaction data. (1471-0064 (Electronic)).

29. Dixon JR, Selvaraj S Fau - Yue F, Yue F Fau - Kim A, Kim A Fau - Li Y, Li Y Fau - Shen Y, Shen Y Fau - Hu M, et al. Topological domains in mammalian genomes identified by analysis of chromatin interactions. (1476-4687 (Electronic)).

30. Hooper JE, Feng W, Li H, Leach SM, Phang T, Siska C, et al. Systems biology of facial development: contributions of ectoderm and mesenchyme. (1095-564X (Electronic)).

31. Liu H, Busch T, Eliason S, Anand D, Bullard S, Gowans LJJ, et al. Exome sequencing provides additional evidence for the involvement of ARHGAP29 in Mendelian orofacial clefting and extends the phenotypic spectrum to isolated cleft palate. Birth Defects Res.

2017;109(1):27-37. Epub 2016/12/29. doi: 10.1002/bdra.23596. PubMed PMID: 28029220; PubMed Central PMCID: PMCPMC5388577.

32. Brinkley JF, Fisher S, Harris MP, Holmes G, Hooper JE, Jabs EW, et al. The FaceBase Consortium: a comprehensive resource for craniofacial researchers. Development. 2016;143(14):2677-88. Epub 2016/06/12. doi: 10.1242/dev.135434. PubMed PMID: 27287806; PubMed Central PMCID: PMCPMC4958338.

33. Hochheiser H, Aronow BJ, Artinger K, Beaty TH, Brinkley JF, Chai Y, et al. The FaceBase Consortium: a comprehensive program to facilitate craniofacial research. Dev Biol. 2011;355(2):175-82. Epub 2011/04/05. doi: 10.1016/j.ydbio.2011.02.033. PubMed PMID: 21458441; PubMed Central PMCID: PMCPMC3440302.

34. Lachke SA, Ho JW, Kryukov GV, O'Connell DJ, Aboukhalil A, Bulyk ML, et al. iSyTE: integrated Systems Tool for Eye gene discovery. Invest Ophthalmol Vis Sci. 2012;53(3):1617-27. Epub 2012/02/11. doi: 10.1167/iovs.11-8839. PubMed PMID: 22323457; PubMed Central PMCID: PMCPMC3339920.

35. Cvjetkovic N, Maili L, Weymouth KS, Hashmi SS, Mulliken JB, Topczewski J, et al. Regulatory variant in FZD6 gene contributes to nonsyndromic cleft lip and palate in an African-American family. Molecular genetics & genomic medicine. 2015;3(5):440-51. Epub 2015/10/06. doi: 10.1002/mgg3.155. PubMed PMID: 26436110; PubMed Central PMCID: PMCPMC4585452.

36. Fakhouri WD, Rhea L, Du T, Sweezer E, Morrison H, Fitzpatrick D, et al. MCS9.7 Enhancer activity is highly, but not completely, associated with expression of Irf6 and p63. Dev Dyn. 2012;241(3):i-i. Epub 2012/02/16. doi: 10.1002/dvdy.23751. PubMed PMID: 22334425.

37. Uslu VV, Petretich M, Ruf S, Langenfeld K, Fonseca NA, Marioni JC, et al. Long-range enhancers regulating Myc expression are required for normal facial morphogenesis. Nat Genet. 2014;46(7):753-8. Epub 2014/05/27. doi: 10.1038/ng.2971. PubMed PMID: 24859337.

38. Visel A, Rubin EM, Pennacchio LA. Genomic views of distant-acting enhancers. Nature. 2009;461(7261):199-205. Epub 2009/09/11. doi: 10.1038/nature08451. PubMed PMID: 19741700; PubMed Central PMCID: PMCPMC2923221.

39. Moreno Uribe LM, Fomina T, Munger RG, Romitti PA, Jenkins MM, Gjessing HK, et al. A Population-Based Study of Effects of Genetic Loci on Orofacial Clefts. J Dent Res. 2017;96(11):1322-9. Epub 2017/07/01. doi: 10.1177/0022034517716914. PubMed PMID: 28662356; PubMed Central PMCID: PMCPMC5607104.

40. Leslie EJ, Mancuso JL, Schutte BC, Cooper ME, Durda KM, L'Heureux J, et al. Search for genetic modifiers of IRF6 and genotype-phenotype correlations in Van der Woude and popliteal pterygium syndromes. Am J Med Genet A. 2013;161A(10):2535-44. Epub 2013/08/21. doi: 10.1002/ajmg.a.36133. PubMed PMID: 23949966; PubMed Central PMCID: PMCPMC3898350.

41. Carlson JC, Taub MA, Feingold E, Beaty TH, Murray JC, Marazita ML, et al. Identifying Genetic Sources of Phenotypic Heterogeneity in Orofacial Clefts by Targeted Sequencing. Birth Defects Res. 2017;109(13):1030-8. Epub 2017/08/02. doi: 10.1002/bdr2.23605. PubMed PMID: 28762674; PubMed Central PMCID: PMCPMC5549861.

42. Beaty TH, Murray JC, Marazita ML, Munger RG, Ruczinski I, Hetmanski JB, et al. A genome-wide association study of cleft lip with and without cleft palate identifies risk variants near MAFB and ABCA4. Nat Genet. 2010;42(6):525-9. Epub 2010/05/04. doi: 10.1038/ng.580. PubMed PMID: 20436469; PubMed Central PMCID: PMC2941216.

43. Gautier L, Cope L, Bolstad BM, Irizarry RA. affy--analysis of Affymetrix GeneChip data at the probe level. Bioinformatics. 2004;20(3):307-15. doi: 10.1093/bioinformatics/btg405. PubMed PMID: 14960456.

44. Ritchie ME, Phipson B, Wu D, Hu Y, Law CW, Shi W, et al. limma powers differential expression analyses for RNA-sequencing and microarray studies. Nucleic Acids Res. 2015;43(7):e47. Epub 2015/01/22. doi: 10.1093/nar/gkv007. PubMed PMID: 25605792; PubMed Central PMCID: PMCPMC4402510.

45. Anand D, Agrawal S, Siddam A, Motohashi H, Yamamoto M, Lachke SA. An integrative approach to analyze microarray datasets for prioritization of genes relevant to lens biology and disease. Genom Data. 2015;5:223-7. Epub 2015/07/18. doi: 10.1016/j.gdata.2015.06.017. PubMed PMID: 26185746; PubMed Central PMCID: PMCPMC4500531.

46. Bolger AM, Lohse M, Usadel B. Trimmomatic: a flexible trimmer for Illumina sequence data. Bioinformatics. 2014;30(15):2114-20. doi: 10.1093/bioinformatics/btu170. PubMed PMID: 24695404; PubMed Central PMCID: PMCPMC4103590.

47. Mathioni SM, Kakrana A, Meyers BC. Characterization of Plant Small RNAs by Next Generation Sequencing. Current Protocols in Plant Biology: John Wiley & Sons, Inc.; 2016.

48. Trapnell C, Pachter L, Salzberg SL. TopHat: discovering splice junctions with RNA-Seq. Bioinformatics. 2009;25(9):1105-11. doi: 10.1093/bioinformatics/btp120. PubMed PMID: 19289445; PubMed Central PMCID: PMCPMC2672628.

49. Pruim RJ, Welch RP, Sanna S, Teslovich TM, Chines PS, Gliedt TP, et al. LocusZoom: regional visualization of genome-wide association scan results. Bioinformatics. 2010;26(18):2336-7. Epub 2010/07/17. doi: 10.1093/bioinformatics/btq419. PubMed PMID: 20634204; PubMed Central PMCID: PMCPMC2935401.

Figure Titles and Legends

Figure 1. Design and analytical strategy to study phenotypic heterogeneity of orofacial clefts. Analyses consisted of four major steps: (1) GWAS for OFC subtypes, (2) selection of SNPs for analysis ($p<10^{-5}$), (3) calculation of heterogeneity Q-statistic p-values and differences in log odds ratios, and (4) plotting each point as a sum of two vectors, each given by the –log10 p-value of the heterogeneity test times the sign of the direction of effect.

Figure 2. Subtype effects for SNPs at representative loci. For each SNP per locus, the effects for CL and CLP, and CLP and CP were compared with heterogeneity Q-statistics. The direction of association was determined by the difference in absolute values of the log odds ratios (i.e. $|\log(OR_{CLP})| - |\log(OR_{CL})|$, $|\log(OR_{CLP})| - |\log(OR_{CP})|$). The coordinates of each SNP were determined by the sum of two vectors, each given by the –log10 p-value of the Q statistic times the sign of the direction. The x-axis of the cleft map represents the CL vs. CLP comparison and the y-axis represents that CLP vs. CP comparison. Concentric circles around the origin based on p-values of the Q-statistics are given for reference (0.01, 0.0001, increasing by 10^{-2}). The centroid of each cluster of SNPs is represented by an “X”.

Figure 3. The Cleft Map. Each of the 29 loci are represented by a single point as the centroid of all SNPs at the locus. The size of the point is scaled to the –log10 p-value for the most significant SNP in the meta-analyses of CL, CLP, and CP. Concentric circles about the origin based on p-values of the Q-statistics are given for reference (0.01, 0.0001, increasing by 10^{-2}). Point size is scaled to represent the best p-value observed in the meta-analyses. Points are colored for clarity of gene name labels.

Supporting Information Captions

Figure S1. Results of genome-wide meta-analyses for (A) cleft lip (CL), (B) cleft lip and palate (CLP), and (C) cleft palate (CP). SNPs with p-values less than 1.00×10^{-5} are highlighted.

Figure S2. **Identifying independent signals with LD clumping.** Results from our previously published CL/P meta-analysis were analyzed with the PLINK [21] clumping procedure (--clump) The clumping procedure takes all SNPs that are significant at the threshold of the index SNPs and forms clumps of all other SNPs that are within 250kb from the index SNP and that are in linkage disequilibrium with the index SNP, based on an r-squared threshold of 0.5. The PLINK clump command is a greedy algorithm so each SNP will only appear in a single clump. To simplify the clumps, we combined clumps. (A) The IRF6 “a” signal consists of only SNPs in “clump 1”; the IRF6 “b” signal consists of SNPs from clumps 2-4. (B) The 8q24 “a” signal consists of SNPs in clumps 1-3; the 8q24 “b” signal consists of SNPs from clumps 4 and 5; 8q24 “c” consists of SNPs from clumps 6 and 7. Panels (C) and (D) show the cleft map plots separately for each clump for IRF6 and 8q24, respectively. Concentric circles indicate significance thresholds for 0.01, 0.001, 0.0001, $1x10x^{-6}$, $1x101x10\times10^{-8}$, 1×10^{-10}, and 1×10^{-12}.

Figure S3. Cleft map for each locus. Concentric circles indicate significance thresholds for 0.01, 0.001, 0.0001, $1x10x^{-6}$, $1x101x10\times10^{-8}$, 1×10^{-10}, and 1×10^{-12}.

Figure S4. Regional association plots for new loci. Results are plotted using the cleft subtype for with the smallest p-values in the genome-wide meta-analyses. Plots were generated using LocusZoom [49]. Symbols are colored by linkage disequilibrium in European populations (1000 Genomes Nov. 2014 release).

Figure S5. Gene expression analysis for genes in Cleft Map loci. For all genes in the topologically associated domains contained Cleft Map SNPs, genes are color-coded based on their craniofacial co-expression module from Hooper et al.

Table S1. Samples used in meta-analyses

Table S2. Results for all SNPs analyzed in the cleft map

Table S3. Genomic coordinates of hESC topologically associated domains overlapping Cleft Map SNPs

Table S4. Expression data for cleft map regions

Table S5. Datasets for SysFACE expression analyses

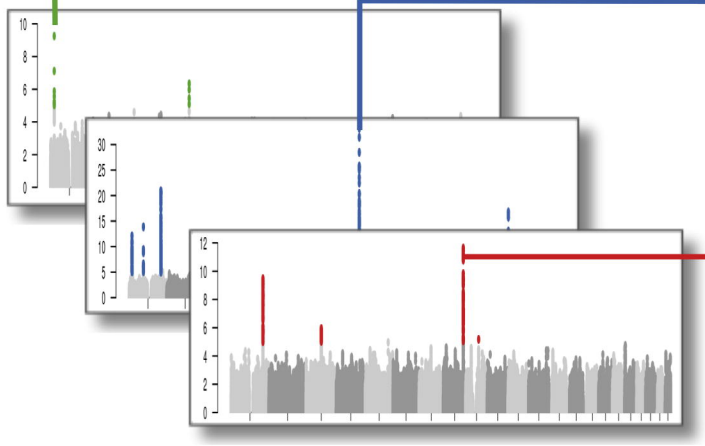

1. GWAS for CL, CLP, or CP

CL	CLP	CP
SNP1	SNP1	SNP1
SNP2	SNP2	SNP2
SNP3	SNP3	SNP3
.	.	.
.	.	.

2. Identify candidate SNPs ($p < 10^{-5}$)

3. Calculate difference in effects

$$Q = \frac{\log(OR_{CL}) - \log(OR_{CLP})}{\sqrt{SE_{CL}^2 + SE_{CLP}^2}} \sim_{approx.} N(0,1) \rightarrow P_{Q1}$$

$$D_1 = |\log(OR_{CLP})| - |\log(OR_{CL})|$$

4. Plot each locus as sum of vector 1 (CL vs. CLP) and vector 2 (CLP vs. CP)

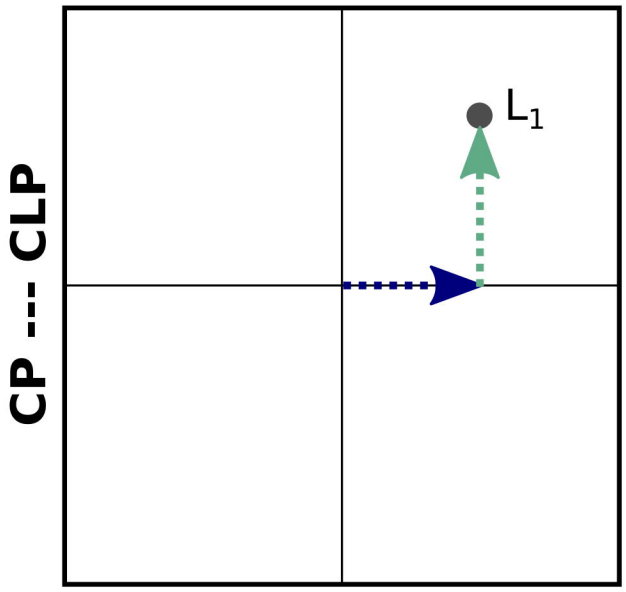

CL vs. CLP			CLP vs. CP		
L_1 { SNP1	P_{Q1}	D_1	L_1 { SNP1	P_{Q2}	D_2
SNP2	P_{Q1}	D_1	SNP2	P_{Q2}	D_2
L_2 SNP3	P_{Q1}	D_1	L_2 SNP3	P_{Q2}	D_2
	.			.	
	.			.	

for each locus (L_n):

$-\log_{10}(P_{Q1}) \times \text{sign}(D_1)$ vector 1

$-\log_{10}(P_{Q2}) \times \text{sign}(D_2)$ vector 2

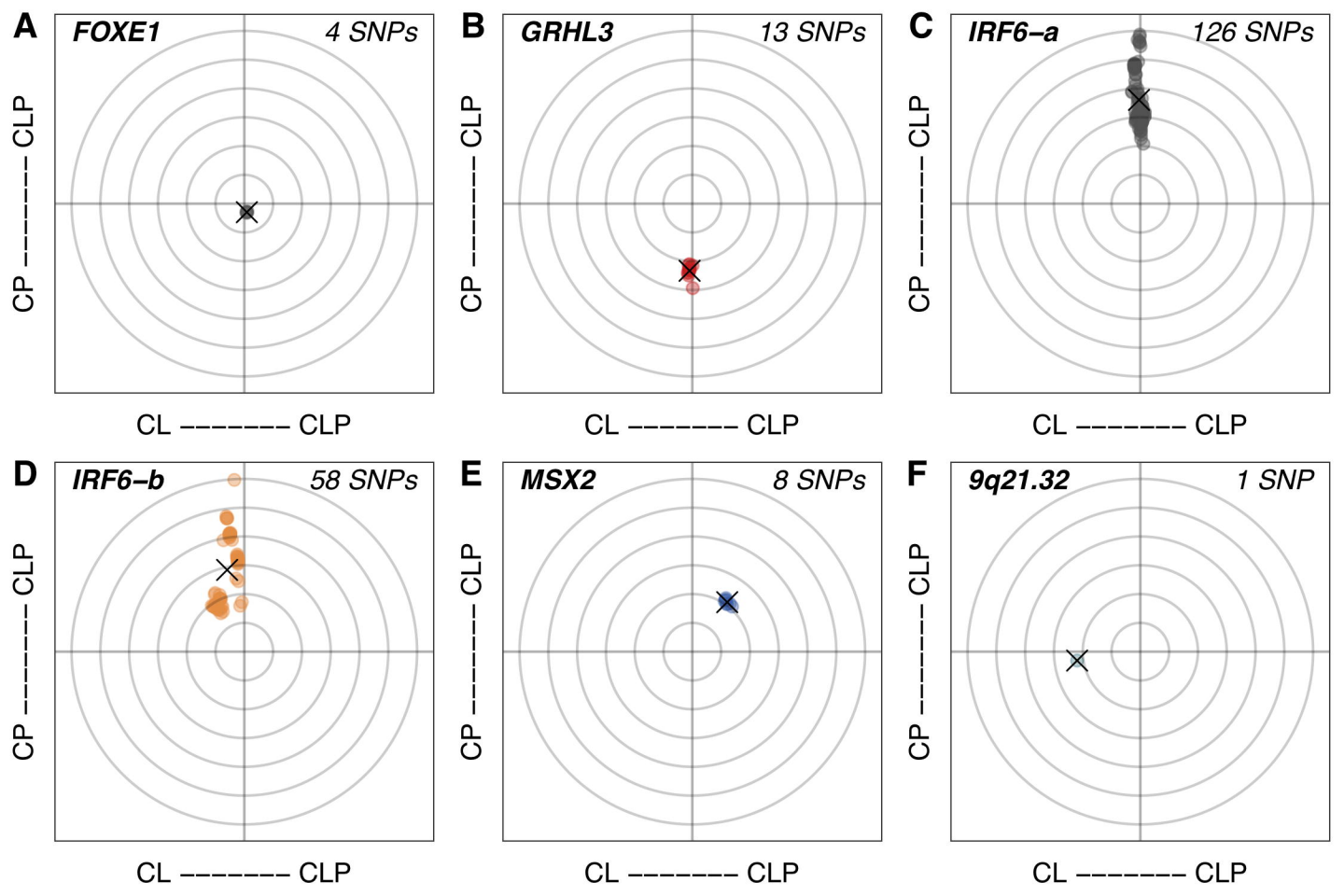
A
FOXE1
4 SNPs
B
GRHL3
13 SNPs
C
IRF6–a
126 SNPs
D
IRF6–b
58 SNPs
E
MSX2
8 SNPs
F
9q21.32
1 SNP
CP ------ CLP
CL ------- CLP

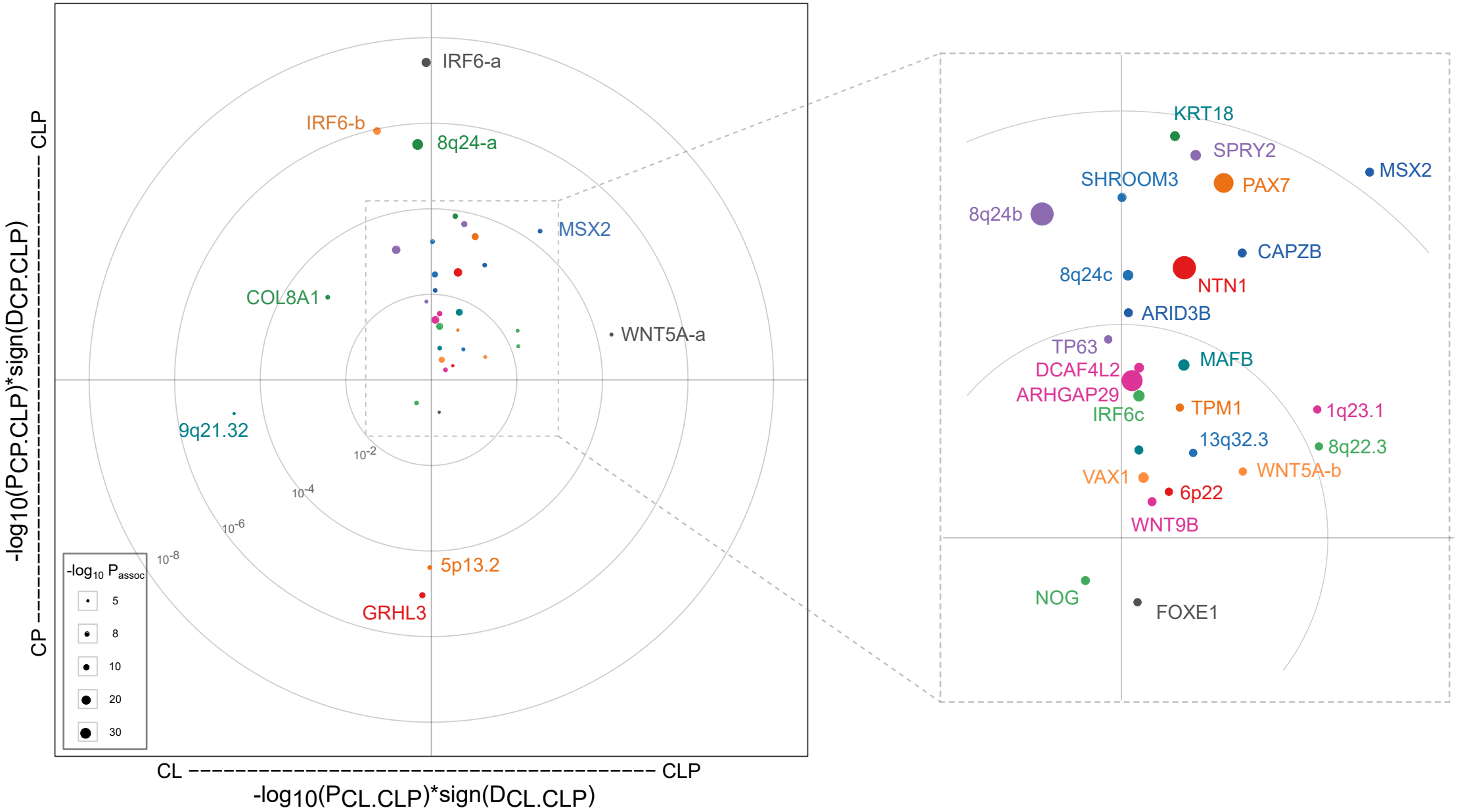
IRF6-a
IRF6-b
8q24-a
MSX2
COL8A1
WNT5A-a
9q21.32
5p13.2
GRHL3
10-2
10-4
10-6
10-8
-log10 Passoc
5
8
10
20
30
CP
CLP
-log10(PCP.CLP)*sign(DCP.CLP)
CL
CLP
-log10(PCL.CLP)*sign(DCL.CLP)
KRT18
SPRY2
MSX2
SHROOM3
PAX7
8q24b
CAPZB
8q24c
NTN1
ARID3B
TP63
MAFB
DCAF4L2
ARHGAP29
IRF6c
TPM1
1q23.1
13q32.3
8q22.3
VAX1
WNT5A-b
6p22
WNT9B
NOG
FOXE1

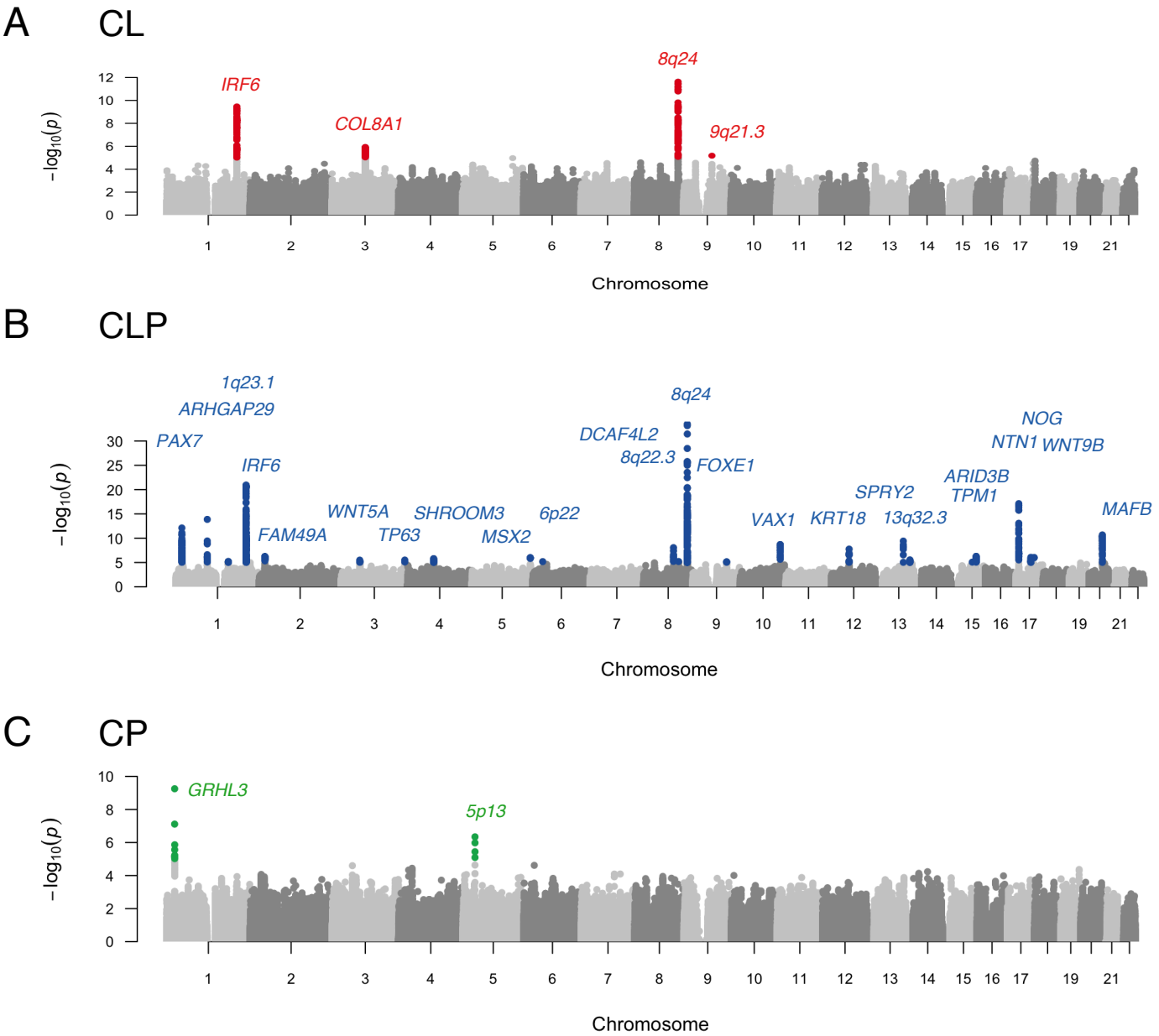
A
CL
IRF6
COL8A1
8q24
9q21.3
−log10(p)
Chromosome
B
CLP
1q23.1
ARHGAP29
PAX7
IRF6
FAM49A
WNT5A
TP63
SHROOM3
MSX2
6p22
8q24
DCAF4L2
8q22.3
FOXE1
VAX1
KRT18
SPRY2
13q32.3
ARID3B
TPM1
NOG
NTN1
WNT9B
MAFB
−log10(p)
Chromosome
C
CP
GRHL3
5p13
−log10(p)
Chromosome

CLP

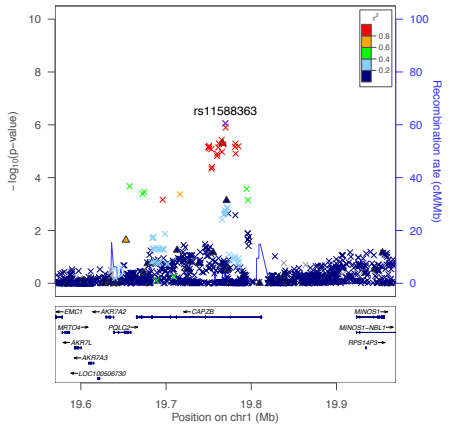
rs11588363
Position on chr1 (Mb)

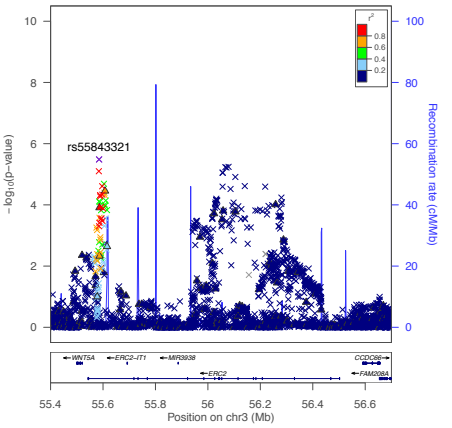
rs55843321
Position on chr3 (Mb)

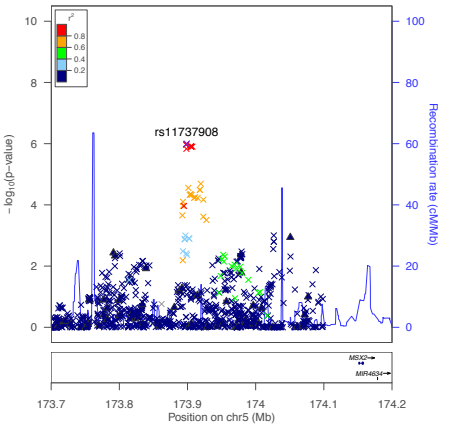
rs11737908
Position on chr5 (Mb)

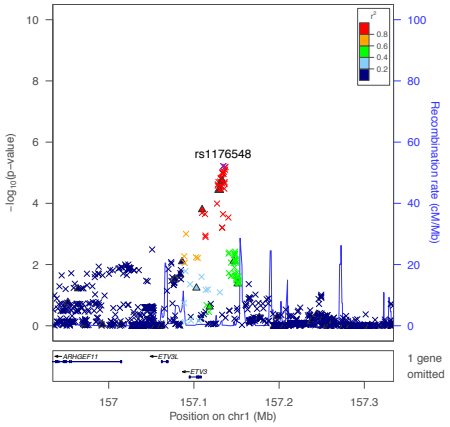
rs1176548
1 gene omitted
Position on chr1 (Mb)

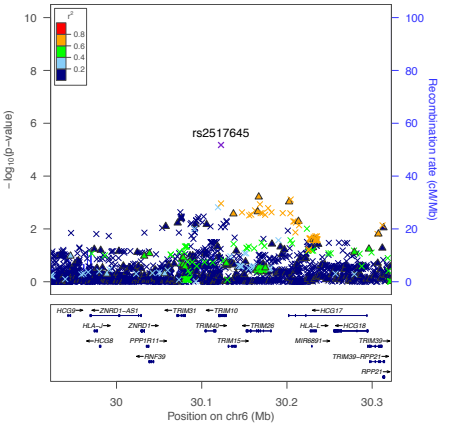
rs2517645
Position on chr6 (Mb)

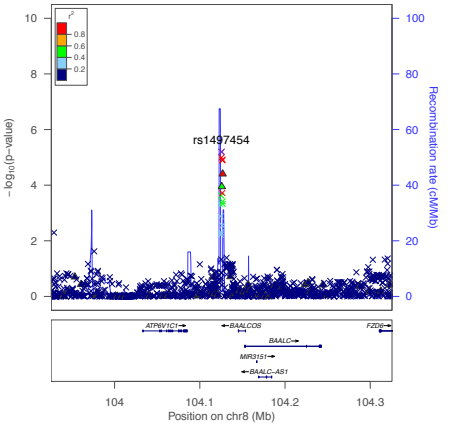
rs1497454
Position on chr8 (Mb)

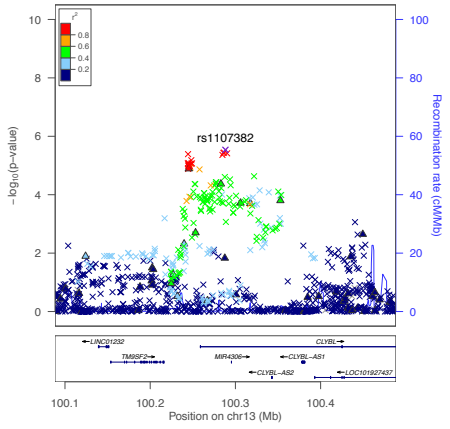
rs1107382
Position on chr13 (Mb)

CP

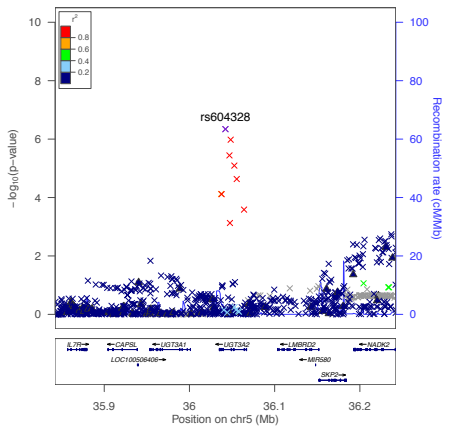
rs604328
Position on chr5 (Mb)

CL

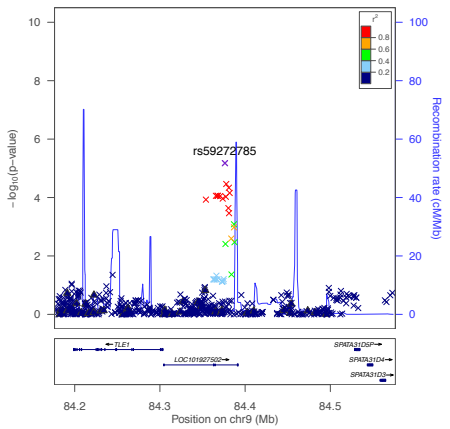
rs59272785
Position on chr9 (Mb)

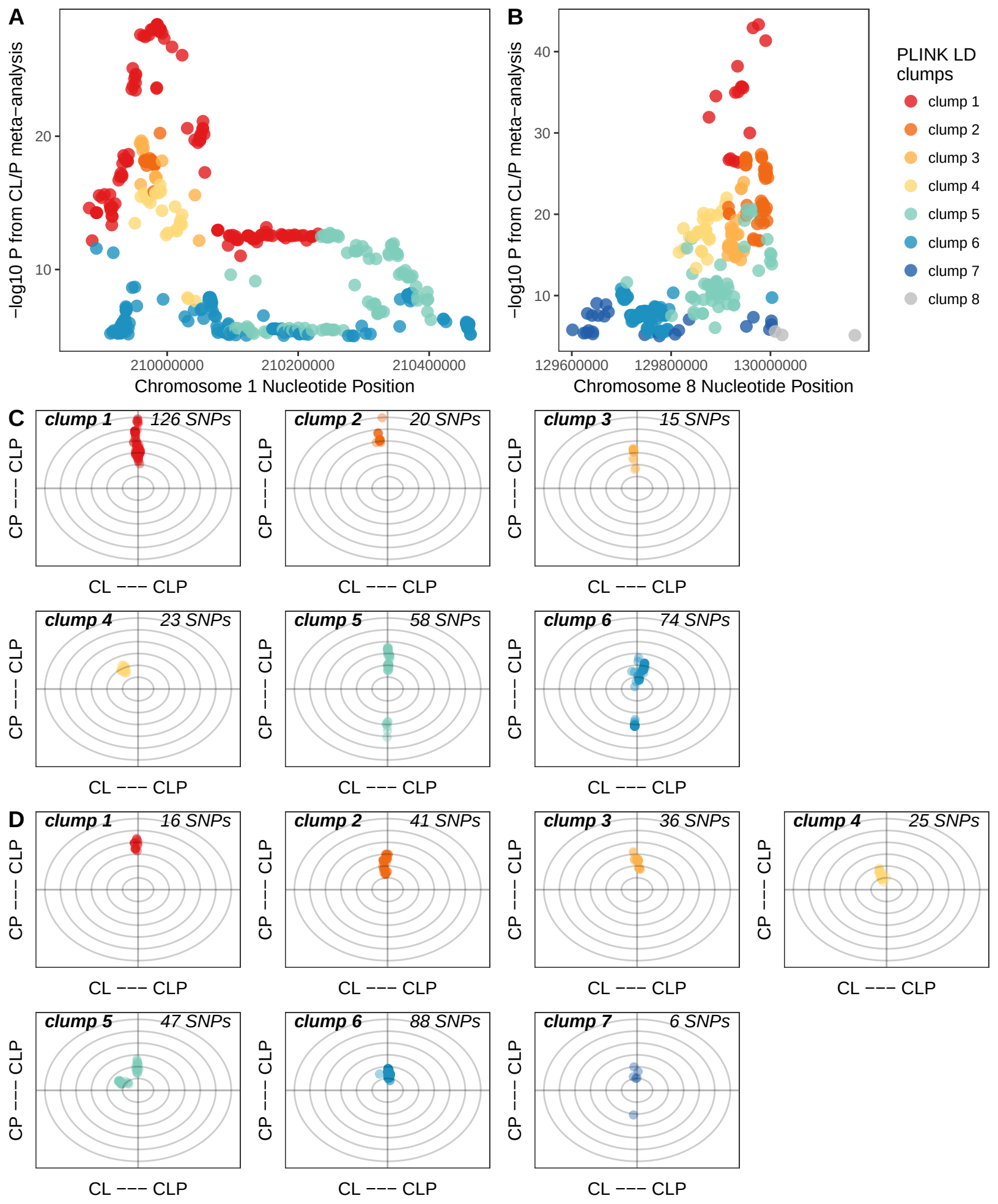
A
−log10 P from CL/P meta−analysis
20
10
210000000
210200000
210400000
Chromosome 1 Nucleotide Position
B
−log10 P from CL/P meta−analysis
40
30
20
10
129600000
129800000
130000000
Chromosome 8 Nucleotide Position
PLINK LD clumps
clump 1
clump 2
clump 3
clump 4
clump 5
clump 6
clump 7
clump 8
C
clump 1 126 SNPs
clump 2 20 SNPs
clump 3 15 SNPs
clump 4 23 SNPs
clump 5 58 SNPs
clump 6 74 SNPs
CP −−− CLP
CL −−− CLP
D
clump 1 16 SNPs
clump 2 41 SNPs
clump 3 36 SNPs
clump 4 25 SNPs
clump 5 47 SNPs
clump 6 88 SNPs
clump 7 6 SNPs

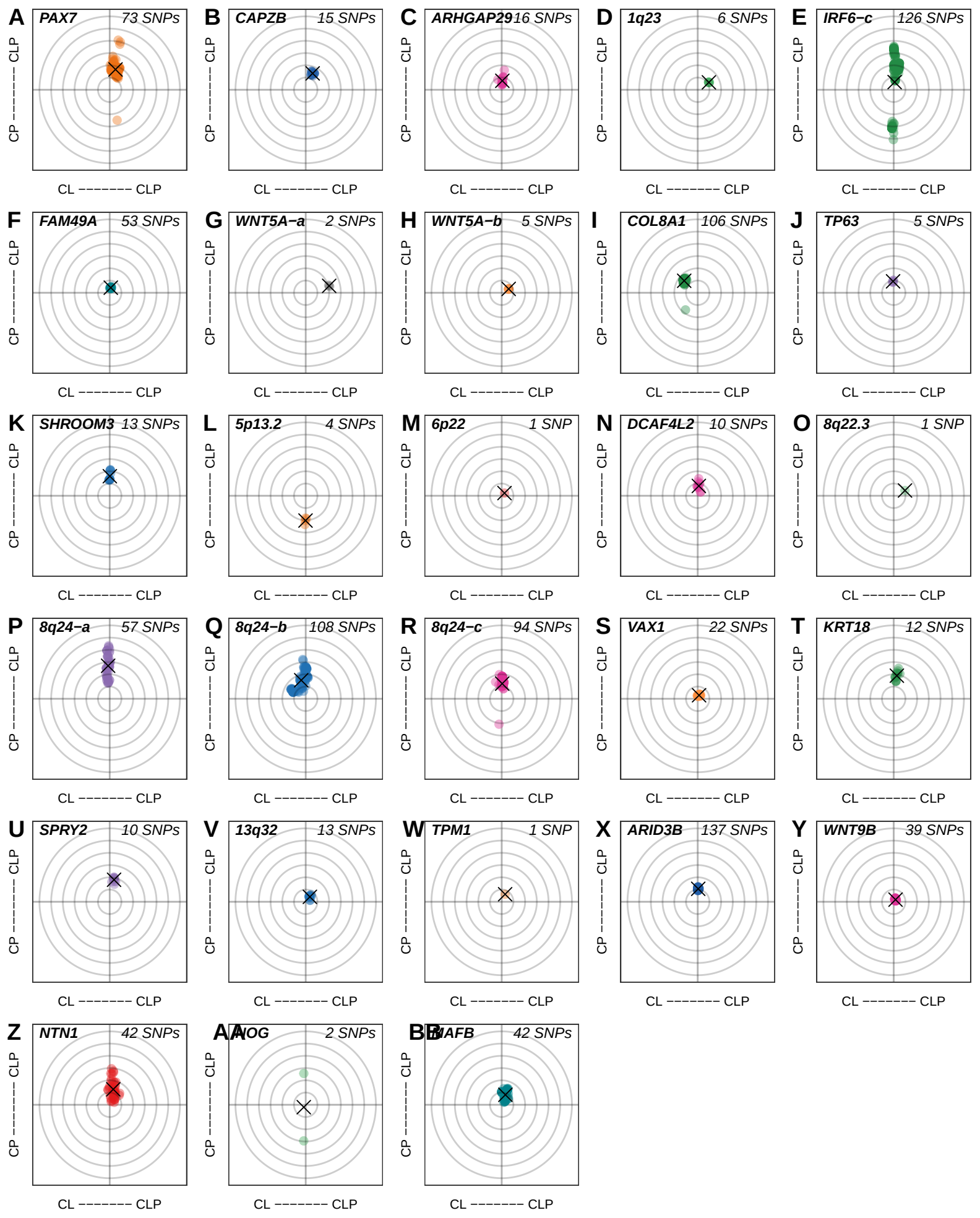
A PAX7 73 SNPs
B CAPZB 15 SNPs
C ARHGAP29 16 SNPs
D 1q23 6 SNPs
E IRF6−c 126 SNPs
F FAM49A 53 SNPs
G WNT5A−a 2 SNPs
H WNT5A−b 5 SNPs
I COL8A1 106 SNPs
J TP63 5 SNPs
K SHROOM3 13 SNPs
L 5p13.2 4 SNPs
M 6p22 1 SNP
N DCAF4L2 10 SNPs
O 8q22.3 1 SNP
P 8q24−a 57 SNPs
Q 8q24−b 108 SNPs
R 8q24−c 94 SNPs
S VAX1 22 SNPs
T KRT18 12 SNPs
U SPRY2 10 SNPs
V 13q32 13 SNPs
W TPM1 1 SNP
X ARID3B 137 SNPs
Y WNT9B 39 SNPs
Z NTN1 42 SNPs
AA NOG 2 SNPs
BB IRF6 42 SNPs
CP ——— CLP
CL ——— CLP

1p36: PAX7

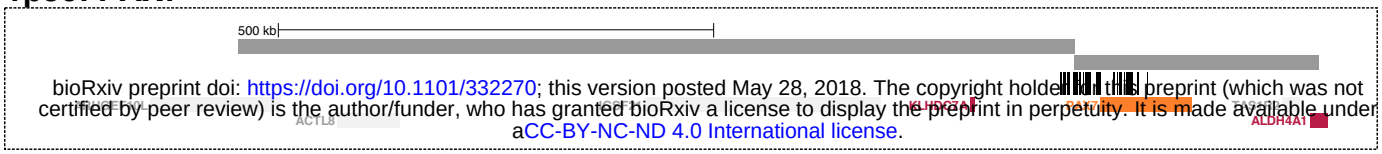

1p36: CAPZB

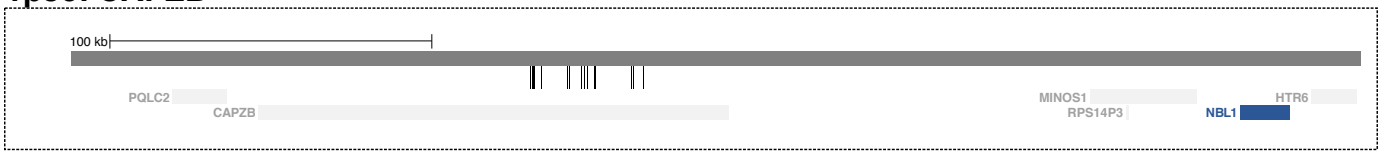

1p36: GRHL3

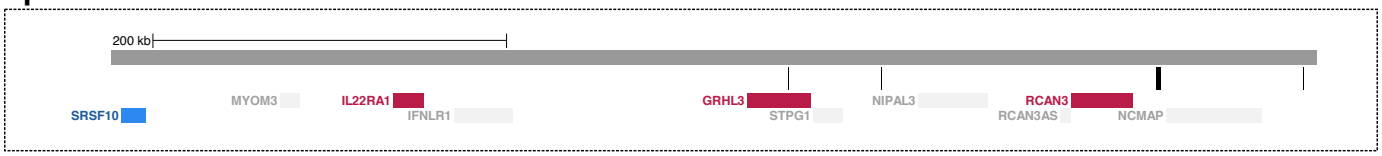

1p22: ARHGAP29

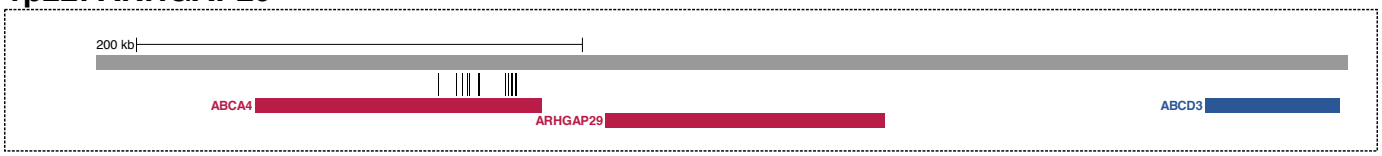

1q23.1

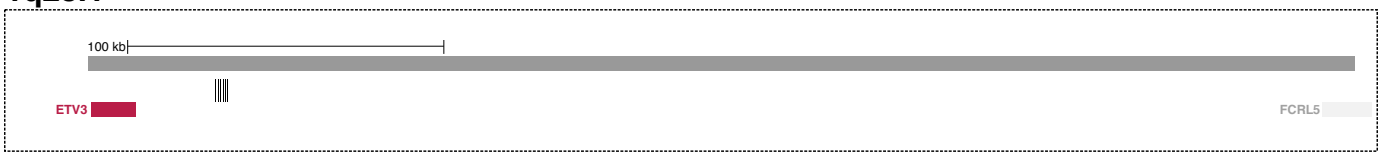

1q32: IRF6

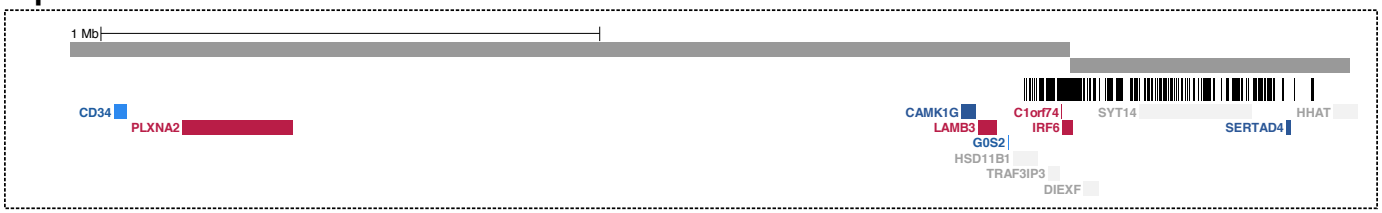

3p14.3: WNT5A

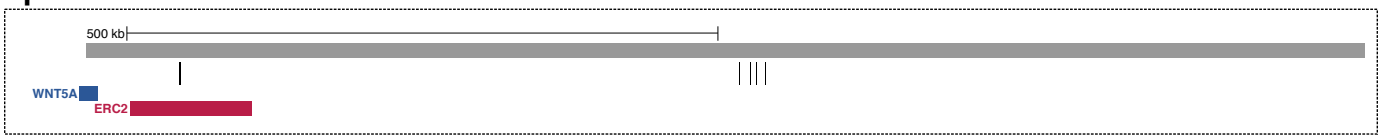

3q12.1: COL8A1

3q28: TP63

4q21.1: SHROOM3

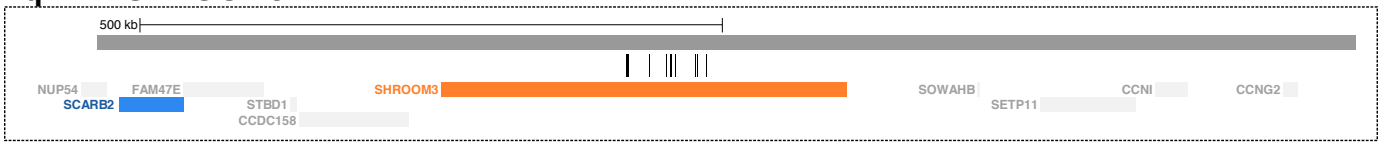

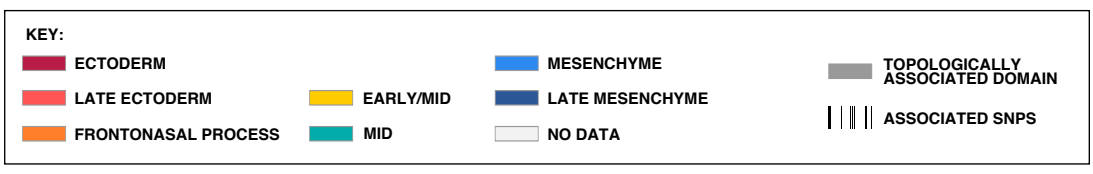

5p13.2

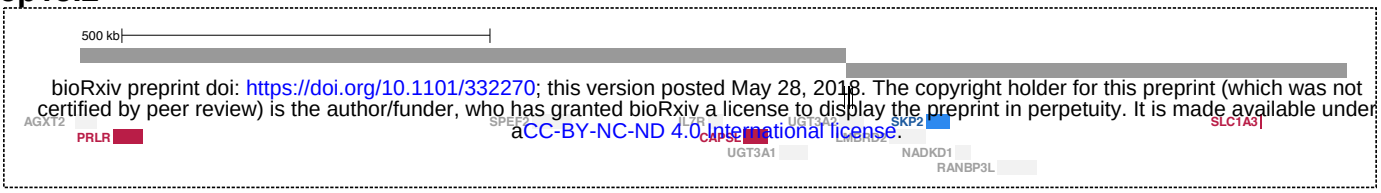

5q35.2: MSX2

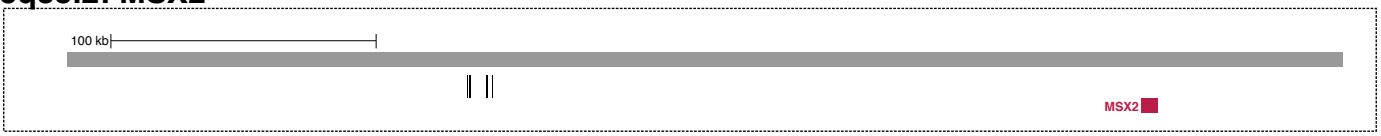

6p22

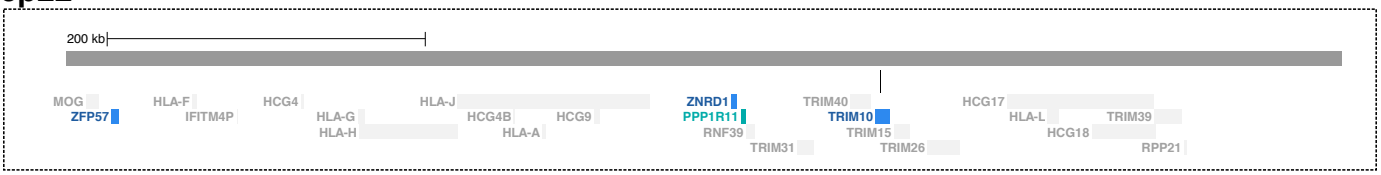

8q21: DCAF4L2

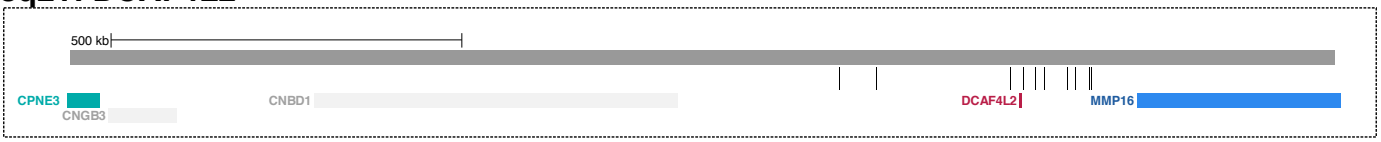

8q22.3

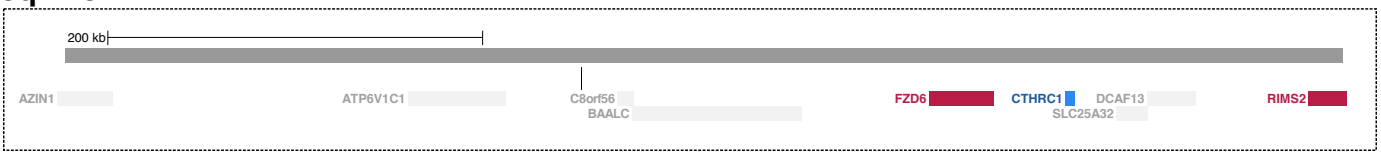

8q24

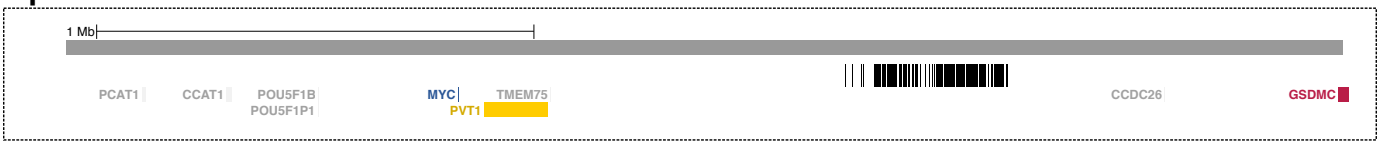

9q21.32

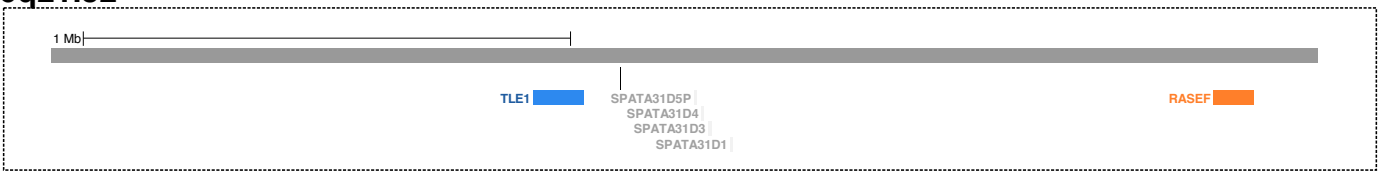

9q22: FOXE1

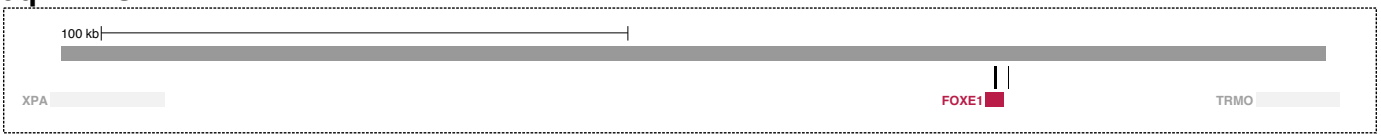

12q13: KRT18

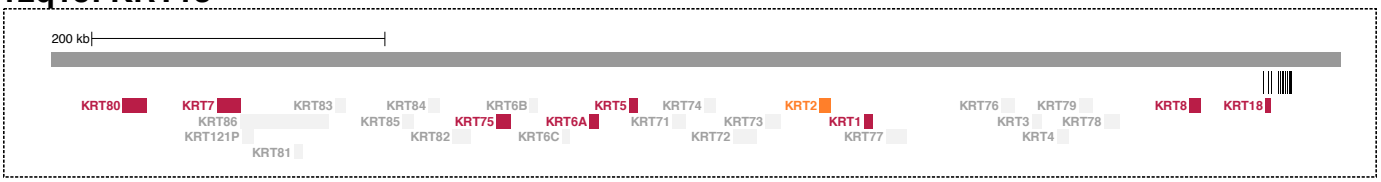

13q31: SPRY2

KEY:

- ECTODERM
- LATE ECTODERM
- FRONTONASAL PROCESS
- EARLY/MID
- MID
- MESENCHYME
- LATE MESENCHYME
- NO DATA
- TOPOLOGICALLY ASSOCIATED DOMAIN
- ASSOCIATED SNPS

13q32.3

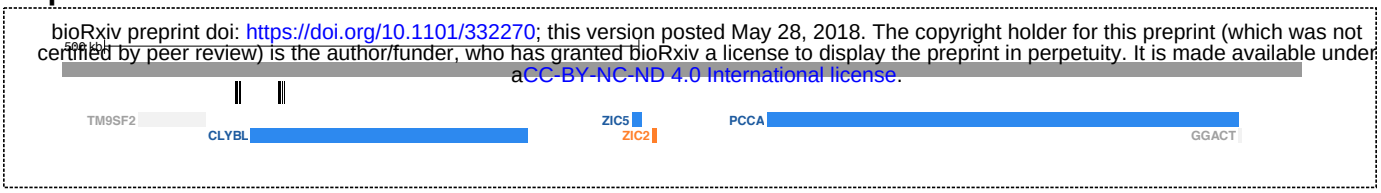

15q22: TPM1

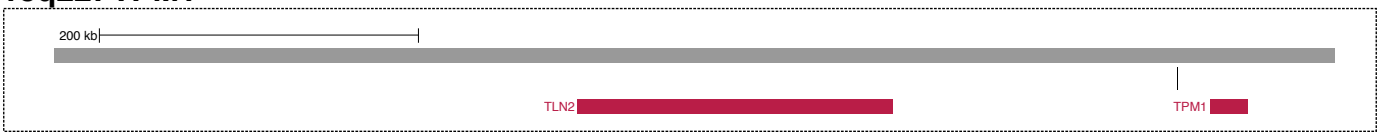

15q24.1: ARID3B

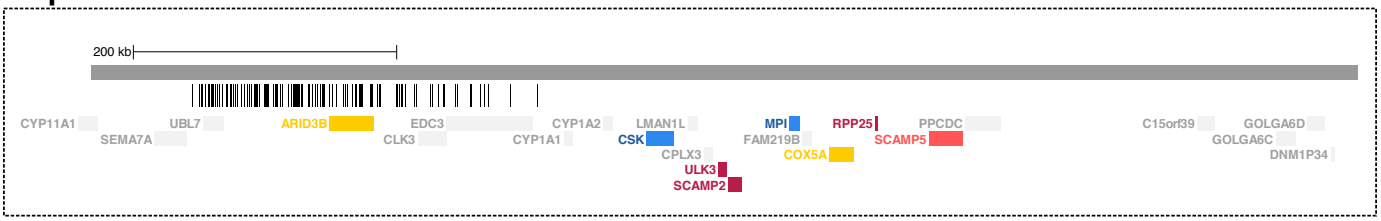

17p13: NTN1

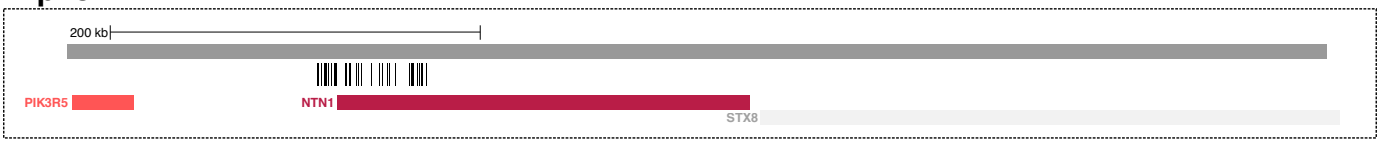

17q21: WNT9B

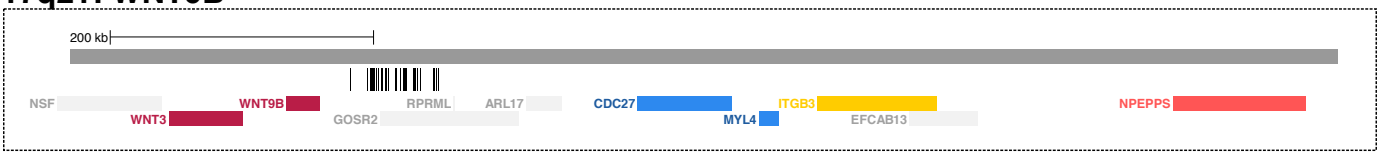

17q22: NOG

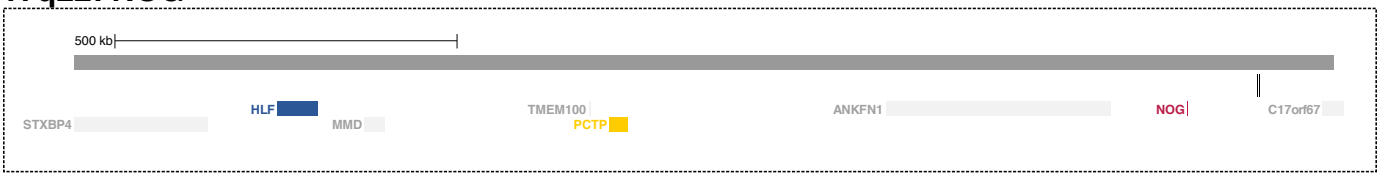

20q12: MAFB

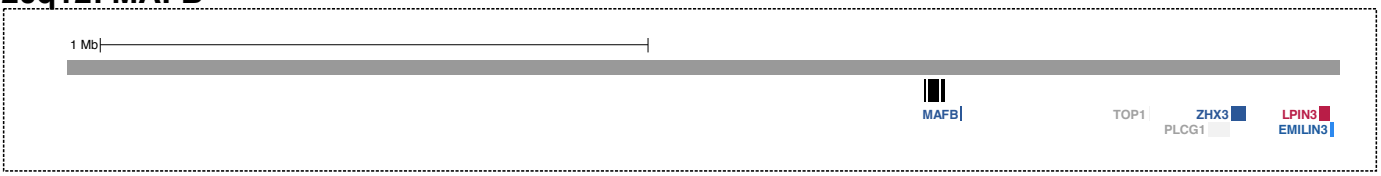

10q25: VAX1